ESPOO 2003 VTT PUBLICATIONS 498

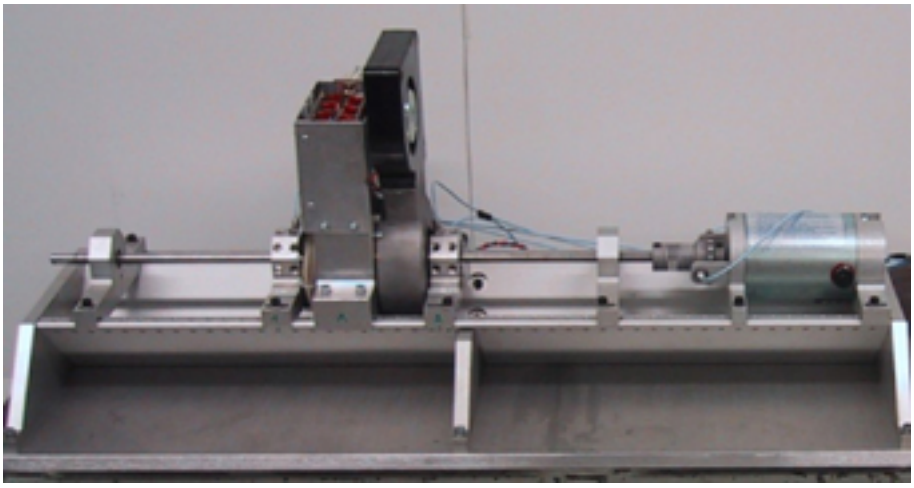

Kari Tammi

Active vibration control of rotor in desktop test environment

VTT PUBLICATIONS 498

Active vibration control of rotor in desktop test environment

Kari Tammi

VTT Industrial Systems

ISBN 951–38–6225–9 (soft back ed.)
ISSN 1235–0621 (soft back ed.)

ISBN 951–38–6226–7 (URL: http://www.vtt.fi/inf/pdf/)
ISSN 1455–0849 (URL: http://www.vtt.fi/inf/pdf/)

JULKAISIJA – UTGIVARE – PUBLISHER

VTT, Vuorimiehentie 5, PL 2000, 02044 VTT
puh. vaihde (09) 4561, faksi (09) 456 4374

VTT, Bergsmansvägen 5, PB 2000, 02044 VTT
tel. växel (09) 4561, fax (09) 456 4374

VTT Technical Research Centre of Finland, Vuorimiehentie 5, P.O.Box 2000, FIN–02044 VTT, Finland
phone internat. + 358 9 4561, fax + 358 9 456 4374

VTT Tuotteet ja tuotanto, Otakaari 7 B, PL 13022, 02044 VTT
puh. vaihde (09) 4561, faksi (09) 456 5888

VTT Industriella System, Otsvängen 7 B, PB 13022, 02044 VTT
tel. växel (09) 4561, fax (09) 456 5888

VTT Industrial Systems, Otakaari 7 B, P.O.Box 13022, FIN–02044 VTT, Finland
phone internat. + 358 9 4561, fax +358 9 456 5888

Technical editing Marja Kettunen

Otamedia Oy, Espoo 2003

Tammi, Kari. Active vibration control of rotor in desktop test environment [Koelaitteiston roottorin aktiivinen värähtelynhallinta]. Espoo 2003. VTT Publications 498. 82 p.

Keywords active vibration control, rotors, test environments, magnetic actuators, modal analysis, damping, measurements, performance, control

Abstract

The goal of this work was to set up a test environment for active vibration control of rotors, to study the dynamics of the system, and to design a control system for controlling rotor vibrations. The principal idea was to use a non-contacting magnetic actuator without a load-carrying function. The test environment consisted of a desktop rotor test rig, a magnetic actuator, and a programmable control unit. The rotor was supported by conventional bearings at the ends, and the control forces were applied at the midpoint of the bearing span. The work reports modal analysis and open-loop measurement results on the test environment. The system was found to vibrate excessively when the rotor was run close to its bending critical speed at 40 Hz. Damping the system, considered as the Jeffcott rotor, by means of a velocity feedback controller was studied. The controller parameters were selected on the basis of estimates derived experimentally from the measured data. According to the simulations and experiments performed, the velocity feedback control system reduced the vibration response significantly. The controller made it possible to run the rotor across the critical speed. Another controller, a feedforward system based on an adaptive finite-impulse-response filter and the use of a reference signal, was designed to compensate disturbances caused by the mass imbalance in the rotor. The filter was adapted by the least-mean-squares algorithm. The simulations and experiments showed that the harmonic response due to the mass imbalance was successfully compensated. The use of the feedback system model improved the performance and extended the operating range of the feedforward system to super-critical conditions. The different roles of the algorithms are pointed out: feedback control increased the damping of the system, while feedforward control compensated the disturbance at the frequency of rotation. The forces required for damping the vibrations were low compared with the mass of the rotor. The use of an adaptive filter led to a considerable reduction in the response, with a minor increase in the active forces used. Results obtained elsewhere in similar test environments are also reported in this work. The data and experience acquired during the construction of the test environment are discussed.

Tammi, Kari. Active vibration control of rotor in desktop test environment [Koelaitteiston roottorin aktiivinen värähtelynhallinta]. Espoo 2003. VTT Publications 498. 82 s.

Keywords active vibration control, rotors, test environments, magnetic actuators, modal analysis, damping, measurements, performance, control

Tiivistelmä

Työn tavoitteena oli rakentaa koelaitteisto roottorivärähtelyjen aktiivisen hallinnan tutkimukseen, määrittää laitteiston dynamiikka ja suunnitella säädin roottorin värähtelyjen vaimentamiseksi. Laitteiston käyttötarkoitus oli tutkia kosketuksettoman toimilaitteen käyttöä perinteisillä laakereilla tuetun roottorin värähtelyjen vaimentamiseen. Koelaitteisto koostui pöytäkokoisesta roottorikoelaitteesta, sähkömagneettisesta toimilaitteesta sekä ohjelmoitavasta ohjainyksiköstä. Koelaitteiston roottori oli liukulaakeroitu päistään, aktiiviset voimat kohdistettiin laakerivälin keskelle. Seuraavaksi esitellään koelaitteistolle tehdyn moodianalyysin sekä avoimen silmukan mittausten tulokset. Tulosten perusteella roottorilla todettiin olevan terävä resonanssi noin 40 Hz taajuudella. Systeemiä approksimointiin Jeffcott roottorina. Systeemin vaste vaimennettiin ensiksi suunnittelemalla takaisinkytketty säädin, jonka parametrit valittiin mitatun datan perusteella. Simuloinnit ja käytännön kokeet koelaitteistolla osoittivat, että roottorin värähtelyvaste pieneni merkittävästi säätimen ansiosta. Säätimen käyttö mahdollisti roottorin käyttämisen lähellä sen kriittistä nopeutta olevilla pyörimisnopeuksilla sallituissa värähtelyrajoissa. Toinen säädin, joka oli myötäkytketty adaptiivinen, suunniteltiin roottorin massaepätasapainosta johtuvan herätteen kompensoimiseksi. Myötäkytkettynä järjestelmänä käytettiin LMS-algoritmilla adaptoitavaa FIR-suodatinta, joka käytti kierrospulssianturilta generoitua sinisignaalia referenssisignaalinaan. Simulointien ja käytännön kokeiden perusteella myötäkytketty algoritmi vähensi roottorin värähtelyvastetta entisestään. LMS-algoritmin versio, joka ei käytä hyväkseen vaimennettavan systeemin mallia toimi alikriittisillä pyörimisnopeuksilla. Takaisinkytketyn järjestelmän mallin lisäys laajensi myötäkytketyn säätimen toiminta-alueen myös ylikriittisille nopeuksille lisäten myös säätimen suorituskykyä. Tutkimuksessa havaittiin algoritmien merkitykset: takaisinkytketty järjestelmä lisäsi systeemin vaimennusta ja myötäkytketty järjestelmä kompensoi herätteen tehokkaasti. Lisäksi havaittiin, että värähtelyjen vaimennus saatiin aikaan pienillä voimilla suhteessa roottorin massaan. Adaptiivisen suodattimen avulla vastetta voitiin pienentää merkittävästi voimien juurikaan kasvamatta. Työssä kuvataan koelaitteisto ja kerrotaan sen rakentamiseen liittyvät asiat. Lisäksi raportoidaan kirjallisuusselvityksen avulla löydetyt vastaavat koeympäristöt.

Licentiate´s thesis

HELSINKI UNIVERSITY OF TECHNOLOGY

Department of Mechanical Engineering

Kari Tammi

Active Vibration Control of Rotor in Desktop Test Environment

Thesis submitted in partial fulfilment of the requirements for the degree of Licentiate of Science in Technology

Espoo April 30, 2003

Inspectors: Professor Mauri Määttänen, DSc (Tech)

Professor Heikki Hyötyniemi, DSc (Tech)

Instructor: Professor Matti K. Hakala, DSc (Tech)

Foreword

This work was carried out at VTT, Technical Research Centre of Finland, Industrial Systems, as a part of a research programme on smart materials and structures called ÄLYMARA. The research programme was started at VTT Manufacturing Technology in 2000, and it continued until the end of 2002. The test environment for active vibration control was constructed in close and fruitful co-operation with High Speed Tech Ltd. The work also benefited from an important contribution from Analog Devices Inc. as a university license of the Visual DSP++ kit.

I wish to thank Professor Petri Kuosmanen, the supervisor of this thesis, and Professor Matti K. Hakala, the instructor of the thesis. Thanks are also due to Mr. Ismo Vessonen and Mr. Pekka Koskinen for an interesting subject and their enthusiasm.

Special thanks are due to Dr. Kai Zenger and Dr. Erkki Lantto for good advice and a very inspiring attitude. Thanks are also due to Mr. Timo Lindroos for creating precise mechanical parts for the test environment. I also thank other colleagues and friends who have contributed to the work.

My parents, Ritva and Martti, deserve my gratitude, for the great support they have given me. Last but not least: Thank you for your love Katja.

Espoo, April 30, 2003

Kari Tammi

Table of contents

Nomenclature

ABBREVIATIONS

AMB	Active magnetic bearings
DAP	Data Acquisition Processor
FIR	Finite Impulse Response filter or non-recursive filter
LMS	Least Mean Squares
PD	Proportional-Derivative
PDD	Proportional-Derivative-Derivative
SDOF	Single Degree of Freedom

SYMBOLS

α	Convergence coefficient
α_{max}	Maximum of convergence coefficient
ε	Eccentricity of rotor
ε_{max}	Maximum allowable eccentricity of rotor
λ	Real and imaginary part of system pole
μ	Convergence coefficient
ω	Angular frequency, or rotational speed
ω_{cr}	Critical speed in radians per second
ω_{max}	Maximum allowable speed in radians per second

ξ	Relative damping
∂	Partial derivative operator
a	Leakage coefficient
c	Damping constant
D	Diameter of active magnetic bearing
$d(n)$	Disturbance signal
e	Neper's number
$e(n)$	Error signal
f_c	Parameter update frequency
f_s	Sampling frequency
F_{ac}	Active force
F_{max}	Maximum active force
F_x	Force in horizontal direction
F_y	Force in vertical direction
$G_m(z)$, $G_m(q)$	Transfer function of model in LMS algorithm
$G_s(z)$	Transfer function of system
h	Sampling time
h_i	Filter coefficient
$H(i\omega)$	Frequency response of Jeffcott rotor in one direction

$H_{av}(z)$	Transfer function of discrete averaging system
$H_{cl}(s)$	Transfer function of continuous closed-loop system
$H_{cl}(z)$	Transfer function of discrete closed-loop system
$H_d(z)$	Transfer function of discrete derivative system
$H_{fb}(s)$	Transfer function of continuous feedback system
$H_{fb}(z)$	Transfer function of discrete feedback system
$H_{ol}(s)$	Transfer function of continuous open-loop system
$H_{ol}(z)$	Transfer function of discrete open-loop system
i	Imaginary unit
i	Phase shift in pulse queue
I	FIR filter order
J	Cost function
k	Spring constant
K_d	Derivative gain
L	Length of active magnetic bearing
m	Mass
m_u	Mass imbalance in Jeffcott rotor
n	Index in pulse queue
p	Pole of system

q	Pulse shift operator
r	Relative speed of rotor
$r(n)$	Filtered reference signal
r_u	Radius of mass imbalance in Jeffcott rotor
Re	Real part operator
s	Laplace variable
t	Time
$u(n)$	Output of FIR filter
V_G	Quality grade for static imbalance
x	Reference signal
X	Horizontal co-ordinate
Y	Vertical co-ordinate
z	Rotor position variable, or variable in discrete time domain
Z	Co-ordinate parallel to rotor shaft

1. Introduction

1.1 Background

The term *active vibration control* generally refers to vibration attenuation or to shifting of the vibration to another frequency band. However, in some applications the amplification of vibrations may be desired. In this work, active vibration control always refers to attenuation of vibrations.

Active vibration control of structures is usually divided into active and semi-active control. In active vibration control, a dynamic force is applied against the vibration to be attenuated. For example, a force-producing member in a structure may compensate vibrations by inducing forces in the structure. In semi-active vibration control, the characteristics of a structure are adjusted in such a way that vibration response is minimised. For example, a component with controllable stiffness may be used. A vibration control system usually consists of one or several actuators, sensors and control units. The sensors provide information on the vibration to be controlled. The control unit is used to realise an algorithm and the actuator is used to apply the control action. Today, one trend is integration of all these functions in the structure, making up an embedded system. Another trend is to develop control systems that can even cope with unexpected operating conditions. Such systems may be called intelligent.

Generally, vibration control in rotating machines is linked to a critical speed, to an excitation at rotation harmonics or to rotordynamic instability. The dynamics of structures are characterised by natural modes. Structures have a tendency to vibrate at their natural frequencies, if excited. A rotating object is subjected to excitation due to gravity, asymmetry, bearings *etc*. The strongest excitation components caused by rotation often occur at frequencies equal to the rotational speed and its sub-multiples and multiples. In this work, the term *critical speed* refers to the speed at which the rotational frequency is equal to the natural frequency of the rotor. As indicated by the term, the critical speed is an issue of great importance for a rotor system. This is because excitation at the natural frequency may cause an excessive response in the rotor. Theoretically with zero damping, the response could increase infinitely. However, damping and non-linearity restrict the response in practice. Some rotor systems can be run at the

critical speed, while others cannot. Usually, heavy rotors are operated below the critical speed, in sub-critical conditions. Light high-speed rotors can be run in super-critical conditions. However, exceptions exist; for example, heavy turbo-generators in power plants work in super-critical conditions. As mentioned above, excitation at rotation harmonics might also cause a problem. For example, the second multiple of the rotational speed excites the rotor already at half the critical speed. A cause for a strong excitation component at second multiple is axial asymmetry in the stiffness of a rotor. Rotordynamic instability is usually associated with the variation of some fluid dynamic pressure around the circumference of the rotor (Vance 1987). This variation can be caused by an interaction between the rotor and its bearings, for example.

The most common active vibration control solution used in rotating machines is the use of active magnetic bearings (AMB). A rotor is levitated in an air gap by actively controlled magnetic forces. Levitating a rotor provides advantages such as low friction and almost maintenance-free operation. AMB have been used in a variety of high-speed applications, from magnetically levitating trains to small electrical machines. AMB solutions are rarer in low-speed applications or in applications where a rotor has to carry large loads or has strong interactions with its environment. For example, a pair of rolls in a nip contact needs to be supported by strong conventional bearings. However, active vibration control is making its debut also in heavy machine design. Some of the possibilities are to control vibrations by means of conventional bearings, to apply a third active bearing, or to change actively the dynamic characteristics of a rotor.

The main purpose of this work was to study how to control vibrations of a rotor supported by conventional bearings by using a supplementary non-contacting electromagnetic actuator. In particular, the work was focused on applications that were not potential AMB applications. This was prompted by the importance of heavy rotating machine manufacturers in Finnish industry. The electromagnetic actuator was chosen because the use of electronics is prevalent in contemporary actuators, sensors, and control systems. The test environment designed is of a small scale and simple. This was found important because basic rotordynamic phenomena can be studied and simple control systems implemented quickly and safely in a laboratory environment. Implementing design methods and control algorithms in a large scale system will require more effort and further research. Nevertheless, this test environment was found to be a perfect start.

The work was carried out in a project included in the 'ÄLYMARA - Smart Materials and Structures' research programme. The research was closely related to the VTT research theme 'Intelligent Products and Systems'. A goal in both research programmes was to introduce intelligent features into conventional machine design.

1.2 Goal

The aim of this work was to construct a test environment for the active vibration control of rotors, to study its dynamical behaviour, and to design and test active vibration control systems. The systems would have to reduce the displacement response in the rotor and extend the operating range of the test system beyond its critical speed. Adaptivity was a property required of the control system to be designed. The test environment was envisaged as a rotor supported by conventional bearings, with control forces generated by a non-contacting auxiliary actuator.

This work was designed to be a step towards the final goal of developing a generic intelligent control system for heavy rotating machines. Therefore, the plan was to study the applicability of the test environment, to relate the results to practice, and to point the way for further research.

1.3 Scope

The active vibration control study was focused on the vibrations in the rotor. The objective was to minimise the displacement in the radial direction in the neighbourhood of the displacement transducers. The actuator, approximately co-located with the transducers, was able to produce a force in the radial direction. The dynamical behaviour of the test environment was tailored to comprise one dominant natural mode. The dynamical behaviour was characterised by a strong response close to the dominant mode; crossing the critical speed was practically impossible without active control.

In the simulations, the rotor was assumed to behave like the Jeffcott rotor: a symmetric massive disk in the middle of a flexible shaft supported by rigid

bearings. The excitation was assumed to be generated by a mass imbalance in the disk. In the controller synthesis, the parameters of the system were assumed to be measurable and time-invariant. Information on the rotational speed of the rotor was available for the compensation of a mass imbalance.

Implementation of the controller was carried out by programming the control algorithms in the C language. The digital signal processor development environment laid down certain boundary conditions for the program (such as sampling rate and number of operations per cycle).

1.4 Contents of this work

The introduction and the literature review constitute Chapter 1. Chapter 2 begins with a description of the test environment, a presentation of the Jeffcott rotor and an introduction to the control algorithms to be used. The results of the identification measurements are then reported. Finally, the designs of the control systems are shown, together with the results of the simulations and the stability checks.

The experimental results are presented in Chapter 3. The control system test results under sub- and super-critical operating conditions are shown, with comparisons between non-controlled and controlled operation. The experimental results together with simulations showed that resonant vibrations in a simple rotor system can be controlled with a velocity feedback controller. The compensation of harmonic excitation due to a mass imbalance with an adaptive filter is also confirmed by the experiments and simulations.

The results are discussed in Chapter 4. The suitability of the test environment is evaluated. The performance and the roles of both control systems are discussed. Chapter 4 also includes some remarks made on the test environment, some practical considerations, and programming issues. Finally, a short summary is presented in Chapter 5.

1.5 Literature review

This literature review starts with a brief introduction of textbooks that may be helpful for further interest. The studies in similar test-benches are then reported. Test-benches consisting of a rotor supported by conventional bearings and an active (or semi-active) vibration control system were of interest. Different actuating methods, actuator placements and scales were used in the test-benches reported. Different control principles were also used, some systems used a reference signal to compensate the disturbances at frequency of rotation, while others did not.

1.5.1 Textbooks

Rotordynamics is discussed thoroughly for example in the textbooks by Vance (1987), Krämer (1993), Genta (1999), and Gasch *et al.* (2002). The principles of active control of mechanical vibrations can be found, for example, in Fuller (1996) or Preumont (2002). The aspects of digital control are presented by Åström & Wittenmark (1990). This book provides important knowledge on the sampling of a continuous-time system and the related digital control. Optimal control is presented by Glad & Ljung (2000). The book discusses the optimality of several control methods. Textbooks on adaptive control have been written by Åström & Wittenmark (1995) and Ioannou & Sun (1996). Active vibration control with magnetic bearings has been studied widely by the control engineering community. Active magnetic bearings are also related to the subject, since the actuator and the control unit were modified from an active magnetic bearing system. A general description of active magnetic bearings can be found in the textbook by Schweitzer *et al.* (1994).

1.5.2 Research on similar test environments

Rotor vibrations were controlled with a magnetic actuator by Cheung *et al.* (1994) at the University of Bath. In the test set-up, the rotor was supported by journal bearings and the control force was applied with a magnetic actuator located at a point within the bearing span. The sliding-mode control method was applied to minimise vibrations due to mass imbalance. The study also included comparative

tests between a fixed-gain PD[1] control and the sliding mode method. The performance of the methods was tested in a test bench with a 2 358-mm-long rotor, 100 mm in diameter. Overhanging disks were attached to the ends of the rotor. The results indicated that sliding-mode control had better performance than fixed-gain PD control. Both control methods gave a large reduction in the response around the critical speed.

An electromagnetic actuator located between the load-carrying bearings was also used by Ishimatsu *et al.* (1991) at the Nagasaki University. The approach was to use an analogue PDD[2] controller to control transients and a digital controller to control the synchronised whirl motion. The control systems worked in parallel. Two different strategies were tested in the digital controller: a heuristic approach, and a neural network approach. The heuristic approach was called the Gain-Phase Modification Method. The method used a reference signal derived from speed measurement and generated a compensation signal by using the displacement error in the output. In the neural network approach, the model of the damper was replaced with a learning neural network. The test set-up consisted of a 460-mm-long rotor, 6 mm in diameter.

A multivariable adaptive self-tuning controller was used to control forced vibrations in a rotor by Sun L. *et al.* (1998) at the University of Melbourne. The researchers used an active hydrodynamic bearing as a third bearing to add damping to the system. The self-tuning regulator was implemented to control oil-film thickness in the third bearing located between the load-carrying ball bearings. The system was designed to cope with non-linear fluid-film bearing characteristics, parameter variations and parameter uncertainty. The simulations indicated that the self-tuning regulator was suitable for forced vibration compensation. The inclusion of a reference signal in the cost function improved the results.

Sliding-mode control and magnetic actuators were also used to damp vibrations in circular saws (Sun J.C. *et al.* 2000) by the National Research Council of Canada. The objective was to reduce vibrations in the saw blade, *i.e.* the vibrations in the

[1] Proportional-Derivative.
[2] Proportional-Derivative-Derivative.

axial direction of a rotor. The tests showed a significant reduction in the cut-width. The system was realised in a sawmill and it is working in a production line. The study is slightly off our focus because it was concerned with axial vibrations rather than radial.

Rotor vibrations have been compensated with a feedforward control system using the convergent control method (Järviluoma & Valkonen 2001, 2002). The study was conducted by VTT and the Helsinki University of Technology. The reference signal used for control was generated from the rotational speed measurement. The test-bench consisted of a large and heavy rotor (diameter 320 mm, length 4 000 mm, weight 800 kg) supported by roller bearings at the ends. The actuating forces, generated by hydraulic cylinders, were applied to the rotor through a third roller bearing. The third bearing was located within the bearing span, close to one end of the rotor, while the objective was to minimise the response at the centre of the rotor. The excitation at the frequency of rotation and its second multiple were successfully attenuated.

The studies presented above used a third point in the rotor for controlling the vibrations. Another approach is to integrate an actuator with a load-carrying bearing. This was done by Ehmann *et al.* (2003) at the Technical University of Darmstadt. A piezo-actuator was integrated with one of two bearings of a rotor. The shaft of the rotor was similar in scale to that used in our study. Two disks were attached to the shaft. Two different controllers were considered: an integral-force-feedback controller and a robust controller designed with μ-synthesis. The use of active control reduced the response of the rotor.

Last, as an example of semi-active control, a magnetorheological fluid damper was introduced a rotor system in (Wang & Meng 2002) at the Shanghai Jiao Tong University. A rotor, 500 mm in length, 9.5 mm in diameter, was supported by two bearings, one of them integrated with the magnetorheological damper. An overhanging disk was attached to the non-drive end of the rotor. The damper was controlled by changing the electrical current through the damper manually. The experiments showed that the damper had an effect on the stability of the rotor.

2. Materials & methods

2.1 Test environment

The leading principle of the study was to control vibrations of the rotor, supported on conventional bearings, by using a magnetic actuator without a load-carrying function. Several rotor kits made for demonstration purposes and research are available on the market. Some of them use conventional bearings, some have active magnetic bearings. However, none of them was exactly what we wanted because the kits with AMB included the electrical components and the control system designed strictly for AMB demonstrations. A possible solution would have been to convert such a magnetic bearing system into an actuator system. However, the modifications required were considered difficult and uncertain, because of their complexity.

In contrast with rotor kits, magnetic actuators with amplifiers and flexible control systems were not commonly available. Our research design required a flexible and effective control system allowing the implementation of different control methods. One approach considered was to construct the control system using commercial servo amplifiers and an I/O card (DAP[3] card) for a personal computer. This approach would have involved a considerable amount of construction work and uncertainty of the final functionality.

A convenient solution was found by using a commercial rotor kit and magnetic actuator controlled with a modified industrial AMB control unit. This combination was found the best in terms of flexibility and functionality. The test environment had to be tailored for the purpose. The critical parts: amplifiers, noiseless signal processing, and performance had already been tested together in industrial use. The Bently Nevada rotor kit RK4 was used. The kit was found easy to modify for our research design. It provided a rotor supported by journal bearings, an electrical drive to run the rotor, displacement transducers to measure the movements of the rotor, and a rigid base, to which any components could be easily attached. The rotor kit was equipped with a magnetic actuator designed for

[3] Data Acquisition Processor.

active vibration control. The design and the manufacture of the actuator were provided by High Speed Tech Ltd, a Finnish company specialising in AMB and high-speed applications. The control unit was provided by the same company. Originally it was type MBC-11, but it was modified for our purpose.

2.1.1 Rotor kit

The rotor kit consisted of a 10-mm-diameter and 560-mm-long rotor supported by journal bearings (Figure 1). The weight of the rotor shaft was 350 g. The rotor is driven by an electrical motor with a separate control box. The desired rotational speed can be selected from 270 rpm to 10 000 rpm. In addition, a rising ramp to the selected speed or a ramp downward can be set from zero up to 15 000 rpm/min. The torque is transmitted from the electrical motor to the rotor by means of a flexible coupling. The radial displacements of the rotor can be measured in two projections with eddy current transducers. The bearings, the displacement transducers, and the electrical motor are all mounted on the V-shaped base in such a way that they are easy to move or detach. The rotor kit also includes two movable or detachable disks that can be fixed to the rotor at any point. These adjustments allowed very straightforward tailoring of the dynamic behaviour of the system.

The common co-ordinate directions were fixed at the beginning of the design process. The Z-axis runs in the axial direction of the rotor towards the drive end. The Y-axis points upwards, perpendicular to the Z-axis. The X-axis is perpendicular to the Z- and Y-axes, satisfying the right hand rule (Figure 1).

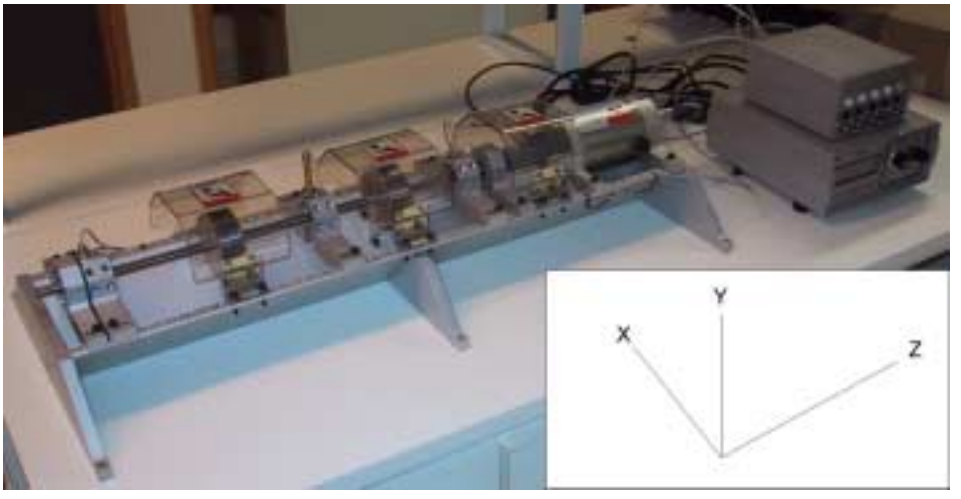

Figure 1. The rotor kit in its basic configuration. The control box and the transducer output box are on the right in the picture. Note the co-ordinate directions used in this work.

2.1.2 Actuator

The body of the actuator was composed of stamped iron sheets joined together by several longitudinal welds on the outer surface. A laminated structure of this kind was used to minimise iron losses in the body as is usual in magnetic circuits. The body had eight teeth forming the iron core for the radially located horseshoe electromagnets. The teeth, pointing to the centre of the actuator, were wound and the windings connected together, forming a hetero-polar actuator, *i.e.* the polarities of the magnets alternated along the circumference. The outside diameter of the body was 100 mm and the inside diameter was 50 mm. The actuator was fixed to the rotor kit body by means of an aluminium mount (Figure 2). The mount was attached to the V-shaped base of the rotor kit in the same way as the bearings and the displacement transducers.

An armature, also a laminated disk pack, was constructed and fixed to the rotor shaft. The actuating forces were induced through the air gap to the armature and the rotor. The outer diameter of the cylindrical armature was 47.5 mm and its length was 65 mm. The part had a conical locking mechanism for low-eccentricity fixing to the rotor. The weight of the armature and the locking mechanism together was 760 g.

Hall transducers were glued onto each tooth in order to measure the magnetic flux density in the air gap. This feature was incorporated in order to measure the force exerted on the rotor. The force can be estimated without information on the flux density if the distance and the coil currents are known. However, the accuracy of the force measurement can be improved with the Hall transducers (Knopf & Nordmann 1998). The readout electronics for the Hall transducers was located on top of the actuator. The signals were fed from the electronics to the control unit.

Figure 2. The actuator body (left) and the mount for the body (right). The read-out electronics and the cable connections were located in the aluminium box on the mount.

The vibration amplitude of the rotor was mechanically restricted to prevent the rotor from hitting the Hall transducers. The dimension budget is shown in Figure 3; the air gap from iron to iron was equal to 1.25 mm in radius. The thickness of the Hall transducers was 0.7 mm and some safety margin (0.25 mm) was required. These figures lead to a maximum allowable displacement of 0.3 mm in radius. A protective bearing was built to restrict the radial vibration amplitude to 0.3 mm (0.6 mm peak-to-peak). The protective bearing, of bronze, was attached to the aluminium mount together with the actuator body. The relatively small safety margin required a good alignment of the actuator with the rotor. The actuator, installed in the rotor kit, is shown in Figure 4.

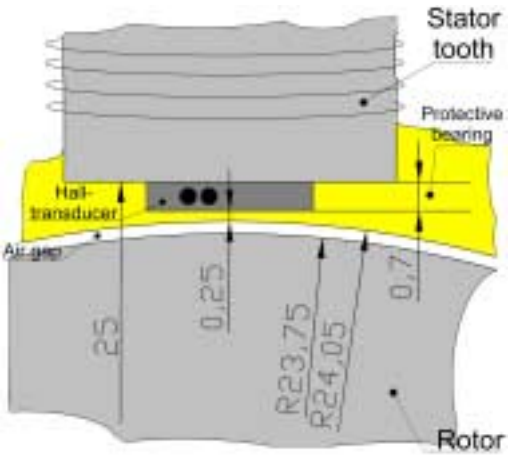

Figure 3. A schematic view of the dimensions between the stator and the rotor. The non-coloured area represents the air gap.

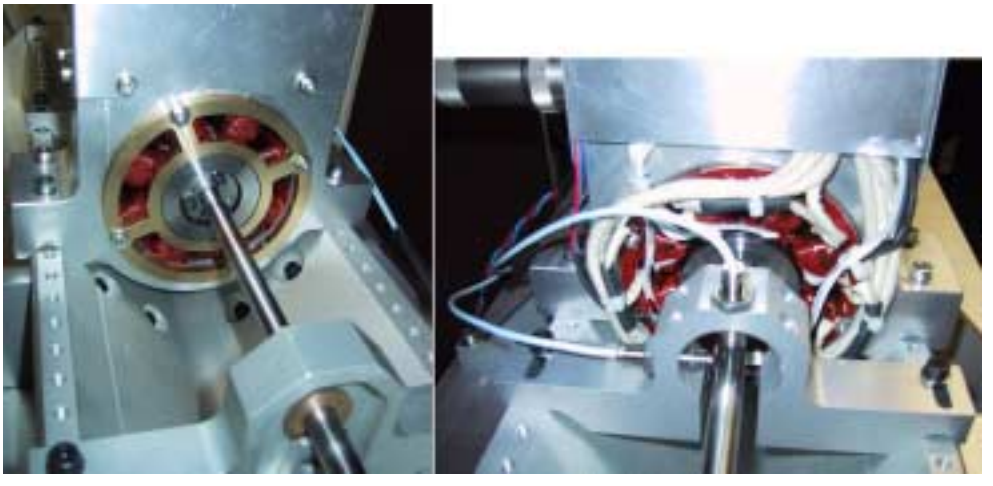

Figure 4. The actuator installed in the rotor kit. Left: the actuator seen from the drive end. The protective bearing is mounted in front of the coils. Right: the actuator seen from the non-drive end. The eddy current displacement transducers are located at the front.

If required, the maximum vibration amplitude could be increased by simply machining the armature in the rotor to a smaller diameter. However, a higher heat dissipation and reduced force production would have to be taken into account if the air gap were to be widened. Cooling the actuator turned out to be an important issue. The small diameter of the rotor led to a compact structure and the specifications required the actuator to produce a high force over a wide frequency band. However, the maximum load of the actuator was not specified accurately because of the inexact knowledge of the magnitude of the forces to be generated. The main reason for the high heat dissipation was the relatively large total iron-to-iron air gap between the metallic components. The 0.7-mm-thick Hall transducers were the main contributors to the magnitude of the air gap. Furthermore, the maximum outer diameter of the actuator was limited by the body of the rotor kit; this restricted the amount of windings used. For these reasons, the system was equipped with a fan and a cooling channel to direct the airflow axially through the actuator (Figure 5).

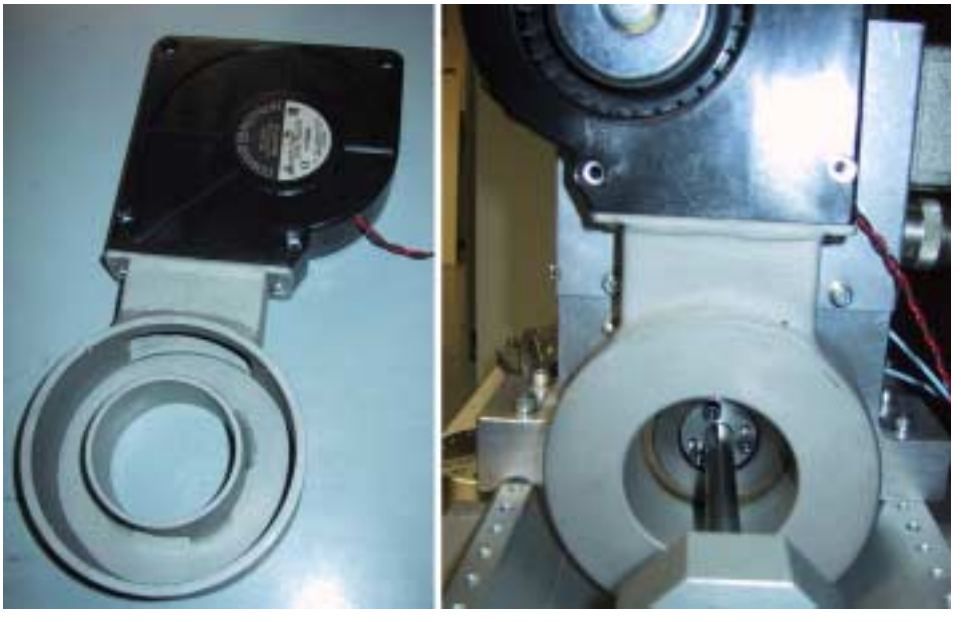

Figure 5. The fan and the cooling channel (left). The actuator seen from the drive end with the cooling system installed (right).

2.1.3 Control unit

The control unit was modified from an active magnetic bearing control system. It is an extensive system for controlling a magnetically levitated rotor comprising four radial and one axial degrees of freedom. Amplifiers for controlling the output currents, programmable signal processing hardware, inputs, and outputs are integrated into the control unit. The whole system including inputs, outputs, signal conditioning systems and amplifiers is run by a digital signal processor. The digital signal processor can be programmed in a personal computer. The software consists of lower-level assembler routines and higher-level C routines. A programmed and debugged control code is first built, linked, then sent into the flash memory, and finally run by the digital signal processor. The system runs autonomously, but it can be connected to a personal computer for debugging and surveillance. For example, variables in the code can be observed, stored and plotted by means of the user interface.

Each magnet in the actuator is driven by one half-bridge amplifier that can generate a current from zero to a maximum value. In other words, the direction of the coil current does not change; each pair of coils is able to exert an attraction force on the rotor. The control unit feeds a constant bias flux density into each magnet; the resulting net force exerted on the rotor is zero. In order to exert a radial force on the rotor, the currents are increased on one side of the actuator and reduced on the other side. (Lantto 1999).

In the modifications, the functions for levitating the rotor were removed from the code because the system was used to control the actuator in our research design. In the control unit, the outputs for driving the actuator currents, communications with a personal computer, and revolution pulse input provided were used as such. The rest of the communication signals were modified for the purpose. Inputs for magnetic field measurement, seven analogue inputs for arbitrary use, and force output signals were added. At least two of these analogue inputs were required for the measurement of the rotor position. The other five inputs were specified as a reserve because the number of inputs may need to be increased in the future. The force output signals, one in the horizontal and the other in the vertical direction, provide a voltage proportional to the measured force, which is computed from the signals provided by the Hall transducers. This output was intended for an external

vibration analyser, if necessary. For example, the frequency response functions of the control unit and the mechanical system can thus be measured separately.

The right point in the code for applying the control algorithms for our purpose was indicated by the supplier. The procedures for producing the control forces were available in the control unit. The control system designed determines the force required and applies the force commands to the force control system (Figure 6). The force control system is run using either flux feedback or current feedback. The flux signals are provided by the Hall transducers; the current signals are measured in the amplifiers.

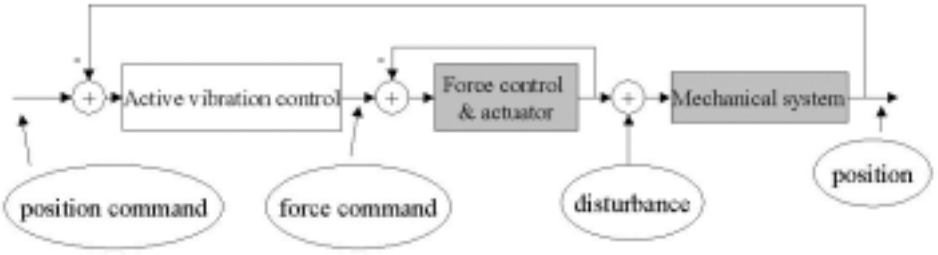

Figure 6. The control unit incorporates the current control, driven in either flux or current feedback mode. The control system applies the force commands to the force control loop.

2.2 Jeffcott rotor

The *Jeffcott rotor* is described by Vance (1987), for example. It consists of a flexible shaft, with zero mass, supported at its ends (Figure 7). The supports are rigid and allow rotation around the centre axis of the shaft. The mass is concentrated in a disk, fixed at the midpoint of the shaft. The system is geometrically symmetric with respect to its rotational axis, except for a mass imbalance attached to the disk. When rotating, the mass imbalance provides excitation to the system.

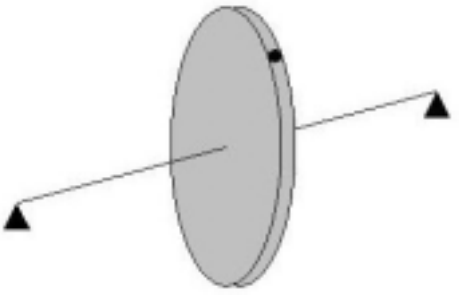

Figure 7. The Jeffcott rotor consists of a shaft, a disk, and a mass imbalance.

For the Jeffcott rotor, the equation of motion is described by

$$m\ddot{z} + c\dot{z} + kz = m_u r_u \omega^2 e^{i\omega t}, \tag{1}$$

where m is the mass of the disk, c is the damping constant representing an external source of damping, k is the spring constant, equivalent to the stiffness of the shaft, and z is the complex variable representing the position of the centre of the disk. The real part and the imaginary part of z can be understood as perpendicular co-ordinate values of the position of the disk. The symbols $\ddot{z}$ and $\dot{z}$ are the second and first time derivatives of the position variable. In the right-hand side, m_u is equal to the unbalancing mass, r_u is the distance of the unbalance from the geometrical centre of the rotor, ω is the rotational speed, i is the imaginary unit, and t is the time variable. In this work, the critical speed is equal to the natural frequency of the Jeffcott rotor[4]. The critical speed in radians per second can be expressed as

$$\omega_{cr} = \sqrt{\frac{k}{m}}, \tag{2}$$

and the relative damping of the system

[4] In the literature, the critical speed is also often defined as the speed at which the maximum response occurs (*i.e.* the damped natural frequency).

$$\xi = \frac{c}{2\sqrt{km}}. \tag{3}$$

With these definitions, Equation (1) can be written

$$\ddot{z} + 2\xi\omega_{cr}\dot{z} + \omega_{cr}^2 z = \frac{m_u}{m} r_u \omega^2 e^{i\omega t}. \tag{4}$$

The Jeffcott rotor was modelled as two separate one-degree-of-freedom systems (Figure 8). They both had equal mass (m), damping (c) and spring constants (k). This consideration was accurate since the Jeffcott rotor was symmetric and no gyroscopic effects occurred. One system was considered to vibrate in the X-plane and the other system in the Y-plane. The responses of these two systems had a phase shift of 90° with respect to each other due to definition of the complex variable z in Equation (1).

The test environment was assumed to represent a Jeffcott rotor. To make this assumption valid, the cylindrical armature was located at the midpoint of the slim shaft. Of course, there were some discrepancies: the bearings had finite stiffness, the shaft had a mass, and the shaft was not perfectly balanced. However, the stiffness of the shaft was assumed dominant compared to the stiffness of the other flexible parts. Similarly, the material concentrated at the centre of the shaft was assumed dominant. The flexible coupling between the electrical motor and rotor was assumed to have a negligible effect. The assumption of the Jeffcott rotor was found a good first approximation. It appeared substantially simple, since it contained one natural mode with no gyroscopic effects. The actuating point of the force and the placement of the displacement transducers were approximately co-located. In practice, the displacements were measured close to the end of the armature fixed to the rotor. This approximation was justified by the fact that most of the deformation occurred in the slim shaft and not in the stiff armature.

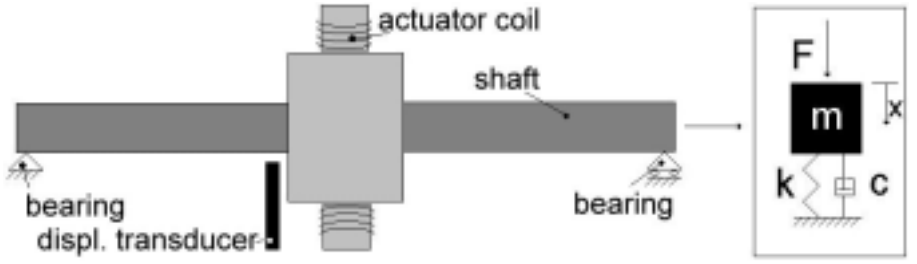

Figure 8. One plane of the rotor-actuator system was simplified to a one-degree-of-freedom oscillator. The other plane formed another similar system.

The response of the oscillator can be expressed as a function of the frequency of rotation

$$H(\mathrm{i}\omega) = \frac{\frac{m_u}{m} r_u \omega^2}{(\mathrm{i}\omega)^2 + \mathrm{i}2\xi\omega_{cr}\omega + \omega_{cr}^2}. \qquad (5)$$

The standards[5] give quality grades for balancing a rotor (Table 1). The grades, usually referred as *G-values*, define a measure of static imbalance as

$$V_G = \omega_{max}\varepsilon_{max}, \qquad (6)$$

where ω_{max} is the maximum allowable angular velocity and ε_{max} is the maximum eccentricity. The eccentricity of a rotor is the distance between the centre of gravity and the centre of rotation (Figure 9).

[5] ISO 1940 standard.

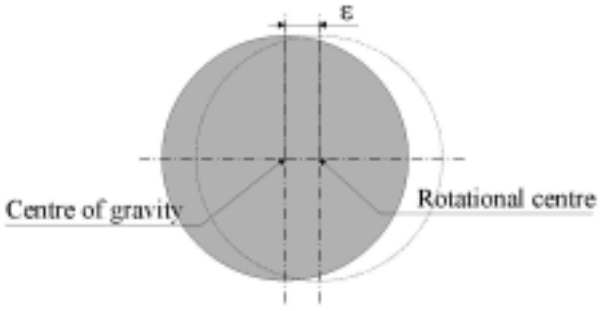

Figure 9. A rotor seen from one end. The eccentricity ε is the distance between the centre of gravity and the centre of rotation.

The mass imbalance (m_u) in the Jeffcott rotor shifts the centre of gravity with respect to the geometrical centre. By introducing the eccentricity, Equation (5) can be modified to

$$H(\mathrm{i}\omega) = \frac{\varepsilon\omega^2}{(\mathrm{i}\omega)^2 + \mathrm{i}2\xi\omega_{cr}\omega + \omega_{cr}^2}, \tag{7}$$

where ε is the eccentricity of the disk in the Jeffcott rotor. Analysis of the response shows that the excitation and the response are equal to zero at zero frequency; in the resonance region the magnitude of the response is defined by the relative damping. At frequencies above the resonance, the absolute value of the response approaches a constant value defined by the eccentricity

$$\left|H(\mathrm{i}\omega)\right| \xrightarrow[\omega\to\infty]{} \varepsilon\,. \tag{8}$$

Figure 10 shows the response as a function of relative frequency with different values of relative damping. The analysis also shows that the response is in the same phase with the excitation at zero frequency. At resonance, the phase of the response is 90° with respect to the excitation. At high frequencies, *i.e.* frequencies significantly higher than the critical speed, the phase is 180°. In other words, the Jeffcott rotor rotates around its centre of gravity at high frequencies; the transition from rotational movement around the geometrical centre to rotational movement around the centre of gravity is called *critical speed inversion* (Vance 1987).

The one-degree-of-freedom oscillator was further analysed in order to clarify what can be achieved with active control. If controlled actively, Equation (4) becomes

$$\ddot{z} + 2\xi\omega_{cr}\dot{z} + \omega_{cr}^2 z = \varepsilon\omega^2 e^{i\omega t} + \frac{F_{ac}(t)}{m}, \tag{9}$$

where $F_{ac}(t)$ is the active force generated by the active control. The optimal way to control the vibrations would be to cancel the excitation completely in such a way that

$$F_{ac}(t) = -m\varepsilon\omega^2 e^{i\omega t}. \tag{10}$$

The following example is to show that active control reduces the response or allows a larger imbalance in the rotor compared with the situation without active control. Let us consider the Jeffcott rotor as a component in a machine. The disk has a weight of 1 000 kg and rotates at a maximum of 3 000 rpm. The maximum eccentricity of the rotor is limited because the response due to mass imbalance is limited to a certain level for functional reasons in the machine. The disk has to be manufactured to a quality grade of 6.3 mm/s in order to fulfil the requirement. Let us then assume that an active dynamic force can be applied to the disk. The sinusoidal force can be controlled in the radial direction and it has an amplitude of 1 500 N. This force is controlled in such a way that the net force acting on the disk is minimised. In this case, the compensation of the excitation reduces the response of the rotor as if it were balanced to a quality grade of 1.5 mm/s. On the other hand, the manufacturing tolerances of an actively controlled rotor can be relaxed. The use of active control allows balancing to a quality grade of 11 mm/s while maintaining response corresponding to a quality grade of 6.3 mm/s in a passive system.

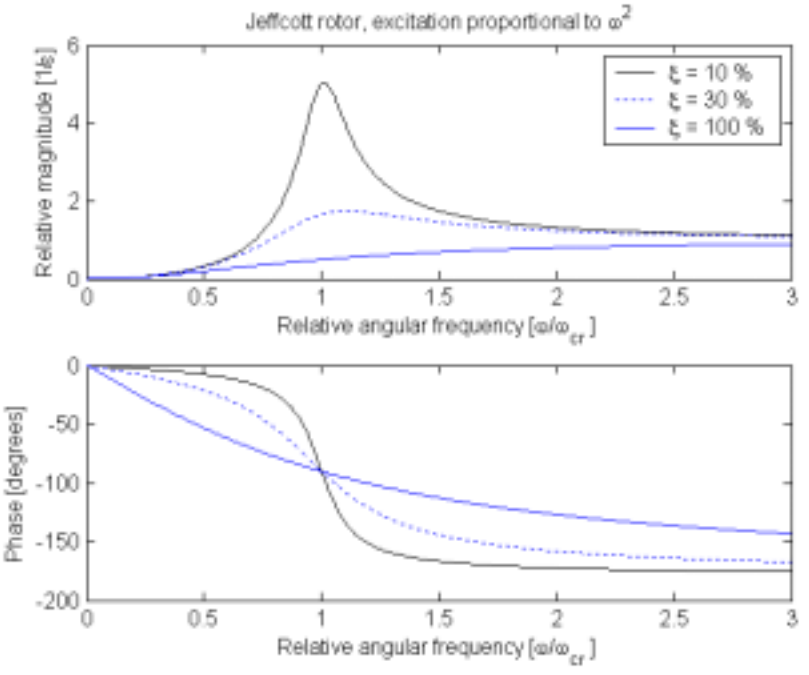

Figure 10. The response of an one-degree-of-freedom oscillator with excitation proportional to the square of the rotational speed plotted for a relative damping of 10 %, 50 %, and 100 %.

As a conclusion, larger imbalance values can be allowed in a rotor if active control is used. Active control may be used to achieve lower production costs, to improve the work-process, to increase the operating range, or to extend the life cycle of the machine. However, supplementary components are always required for active vibration control. These components cause additional cost, require design and need maintenance. Hence, the use of active control is a trade-off between the benefits and required extra effort. The example assumed a sinusoidal radial force with an amplitude of 1 500 N. In the case of active magnetic bearings with traditional silicon steel laminates, the maximum force can approximately be derived from the bearing dimensions:

$$F_{max} \approx LD \cdot 20 \frac{\mathrm{N}}{\mathrm{cm}^2}, \qquad (11)$$

where L is the length of the magnetic bearing and D is the diameter of the rotor at the bearing (Lantto 1999). This indicates that the required dimensions are perfectly realistic for a 1 000 kg rotor; the force can be realised with the bearing dimensions L = 75 mm and D = 100 mm.

Table 1. Quality grades recommended for different types of rotors (ISO 1940, Genta 1999).

Quality grade [mm/s]	**Rotor type**
40	Car wheels, wheel rims, drive shafts. Crankshaft/drives of engines of cars, trucks and locomotives
16	Drive shafts (propeller shafts, cardan shafts) with special requirements. Parts of agricultural machinery. Individual components of engines for car, truck and locomotives
6.3	Parts of process plant machines. Paper machinery rolls; print rolls. Fans. Assembled aircraft gas turbine rotors
2.5	Gas and steam turbines, including marine main turbines. Rigid turbo-generator rotors. Turbo-compressors
1	Tape recorder and phonograph drives. Grinding machine drives. Small electric armatures with special requirements

2.3 Control system design

The control systems to be used are presented in Sections 2.3.1 and 2.3.2. The design of the control system was divided into two parts. First, a velocity feedback control system was used to reduce the system response over a wider frequency band. The modification could be interpreted as a manipulation on the left-hand side of the Equation (1). Actually, the active force does not change the

mechanical characteristics of the system, but it works roughly as if the damping of the system were increased. Second, a feedforward system was used to compensate the excitation. This was done by using an adaptive filter to create a force counteracting the mass imbalance. The compensation can be interpreted as a manipulation in the right-hand side of the Equation (1).

2.3.1 Feedback control

For a one-degree-of-freedom oscillator, the transfer function from a force to displacement can be expressed as

$$H_{ol}(s) = \frac{1}{ms^2 + cs + k}, \tag{12}$$

where s is the Laplace variable, m corresponds to the vibrating mass, c is the damping constant and k the spring constant. The function $H_{ol}(s)$ refers to an open-loop transfer function, *i.e.* the response of a non-controlled system. For a system with low damping, the maximum response occurs at the resonance frequency, and its magnitude is inversely proportional to the damping constant. The velocity feedback, shown in Figure 11, continuously measures the displacement at the output and creates a force opposed to the vibration velocity at any instant of time. Thus, the transfer function for the velocity feedback control system is

$$H_{fb}(s) = K_d s \quad , \tag{13}$$

where K_d is the derivative gain. For the controlled system, the closed-loop transfer function with velocity feedback becomes

$$H_{cl}(s) = \frac{1}{ms^2 + (c + K_d)s + k} \ . \tag{14}$$

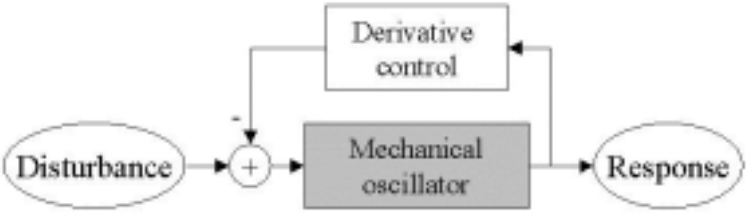

Figure 11. The velocity feedback system produces a control action proportional to the time derivative of the displacement.

The response magnitude at resonance region can be determined by selecting an appropriate derivative gain. Selecting a positive number for the derivative gain is then equivalent to adding external damping to the rotor system. The system poles are defined as the roots of the characteristic equation (the roots of the denominator of the closed-loop transfer function). The poles characterise the behaviour of a system. The system is stable if the real parts of all the system poles are less than zero. A mechanical system is called critically damped if the poles are located on the negative real axis at -1. For example, the requirement for the poles of the closed-loop system

$$p = -\lambda - \mathrm{i}\lambda\,, \tag{15}$$

and

$$\overline{p} = -\lambda + \mathrm{i}\lambda\,, \tag{16}$$

where λ is a positive constant and i is the imaginary unit, is a common way to place closed-loop poles, leading to a good behaviour of the closed-loop system (Glad & Ljung 2000). This corresponds to the relative damping

$$\xi = \frac{1}{\sqrt{2}}\,. \tag{17}$$

Using the requirement in Equations (15) and (16) and solving the derivative gain from the characteristic equation yields

$$K_d = \sqrt{2mk} - c\,. \tag{18}$$

In principle, all the parameters have to be known to compute the gain accurately. However, the damping constant of a mechanical system is usually small in comparison with other parameters, and could thus be neglected. The modal mass and stiffness can be computed from the natural frequency and the static gain of the system. Static gain is the response at zero frequency.

Since the test environment system is computer controlled, the control system was discretised. Using the forward difference approximation, the pulse transfer function of a discretised system is

$$H_d(z) = K_d \frac{z-1}{h}, \tag{19}$$

where z is the variable in the discrete time domain and h is the sample time. Differentiation as an operation is prone to high-frequency noise. A low-pass filter was designed, to restrict the control action to a certain bandwidth[6]. Maybe the simplest low-pass filter is the averaging filter, which gives the average of two successive samples as the output. Its pulse transfer function is

$$H_{av}(z) = \frac{z+1}{2z} \quad . \tag{20}$$

The mechanical system must also be discretised for the analysis. The zero-order-hold method was used for discretisation because control signals are held constant between successive samples in the control unit.

The operation during one control period can be expressed verbally as follows:

1. Measure the current displacement

2. Save the displacement for the next control period.

3. Compute the difference of two successive samples.

---

[6] Naturally, the bandwidth of the counter-force was also limited by the bandwidth of the actuator.

4. Compute the control force, multiply the difference by the overall gain taking into account the derivative gain, the sample time, and the transducer sensitivity.

5. Save the force for the next control period.

6. Compute the average of two successive control forces.

7. Send the average to the force controller.

2.3.2 Feedforward control

Feedforward systems are based on the use of a reference signal to compensate a disturbance. The reference signal may be a measured disturbance or a signal correlating with the disturbance. In adaptive feedforward systems, an error signal is used to adapt the system. The error signal, the difference between the desired output and the actual output, it to be minimised by means of adaptation. For example: in active sound control, the disturbing noise signal may be measured before it enters the controlled volume and used as a reference signal. The difference between the desired sound and actual measured sound in the controlled volume may be used as the error signal to be minimised.

For the Jeffcott rotor, its mass imbalance is the only source of excitation. For real rotors, mass imbalance is one of the largest sources of excitation. Hence, a significant part of the excitation can be compensated by compensating the disturbance caused by the mass imbalance. The imbalance compensation in active systems can be performed by feeding a sinusoidal counter-force, acting against the imbalance force, into the system. Accurate measurement of the imbalance, its magnitude and phase, as a function of rotational frequency may be difficult in a rotating machine. However, the frequency of the disturbance due to imbalance is often known because the rotational speed is commonly measured in rotating machines. The rotational speed measurement provides a possibility to generate a reference signal that has the same frequency as the disturbance due to imbalance. If the position error of the rotor is also measured, an adaptive feedforward system may be used. The problem is then to estimate the correct amplitude and the correct phase with respect to the mass imbalance in order to create a compensating counter-force.

Figure 12 shows a feedforward system connected in series with the feedback system. The system consists of a feedforward control and a mechanism to adjust its parameters in order to achieve the correct gain and the correct phase between the reference and the disturbance.

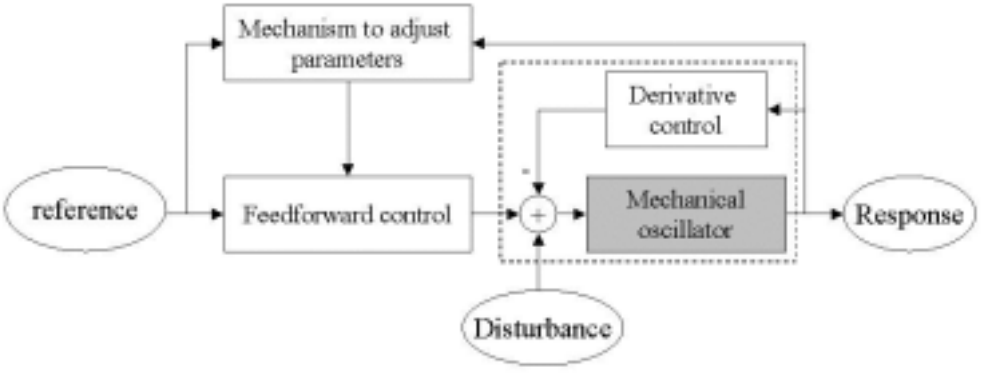

Figure 12. A feedforward system for compensating the excitation due to mass imbalance. The feedforward block feeds a compensating signal to the velocity feedback system (inside the dashed line).

Consider the system shown in Figure 13, the objective is to minimise the absolute value of the output signal $e(n)$. The system is subjected to the disturbance $d(n)$, which is to be compensated by filtering the reference signal $x(n)$. The optimal FIR[7] filter minimises the mean square error. The output of the filter, $u(n)$, is a sum of I pieces of input pulses multiplied by the weighting coefficients h_i

[7] Finite Impulse Response or non-recursive filter.

$$u(n) = \sum_{i=0}^{I-1} h_i \cdot x(n-i)\,, \tag{21}$$

where $x(n)$ is the input sequence, I is the order of the filter, and n is the index pointing to the latest input. The sequences are formed of real rather than complex signals. (Fuller *et al.* 1996, Elliot 2001).

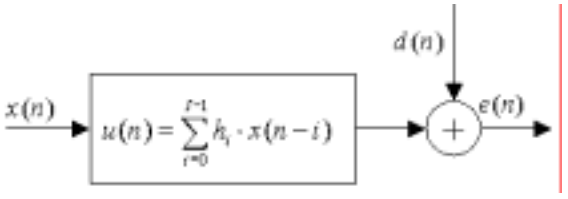

Figure 13. The reference signal x(n) is to be filtered in such a way that the absolute value of the output e(n) is minimised.

To minimise the absolute value of the error, a quadratic cost function is defined as

$$J = e^2(n)\,. \tag{22}$$

Consider the cost function as a function of the filter coefficients; if any of the coefficients takes a large positive or a large negative value, the quadratic function J becomes large. Thus, the cost function always has a minimum rather than maximum and the optimal set of the coefficients leads to the minimum value of the cost function. This minimum is unique if the reference signal consists of at least half as many frequencies as the filter has coefficients. The reference signal is then said to be *persistently exciting*. The optimal coefficients may be computed by using the autocorrelation properties of the reference signal and the cross-correlation between the reference and desired signal. However, a considerable amount of data and computational effort are required to solve the optimal set of coefficients. (Elliot 2001).

An alternative solution to finding the optimal coefficients is to develop an adaptive filter. In the adaptive filter, the coefficients are adjusted sequentially in such a way that the mean square error converges towards to the minimum. Each new set of data is used to re-adjust the coefficients that are converging towards the optimal coefficients. One suggestion for updating the coefficients is the

steepest-descent algorithm. The coefficients are updated in the negative direction of the local gradient of the cost function

$$h_i(n+1) = h_i(n) - \mu \frac{\partial J}{\partial h_i}(n), \tag{23}$$

where μ is the convergence coefficient. The convergence coefficient has to be a small positive number in order to ensure stability of the algorithm. Widrow and Hoff proposed that the partial derivative of the cost function with respect the coefficients may be computed as the derivative of the instantaneous error with respect to the coefficients

$$\frac{\partial J}{\partial h_i}(n) = 2e(n)x(n-i). \tag{24}$$

By combining the Equations (23) and (24) the weighting coefficients are updated according to

$$h_i(n+1) = h_i(n) - \alpha e(n)x(n-i), \tag{25}$$

where $\alpha = 2\mu$ is another convergence coefficient. This update law is known as the *LMS algorithm*[8]. (Elliot 2001).

In Figure 12, the error to be minimised is measured at the output of the oscillator, not at the output of the FIR filter. Depending on the dynamics of the system, the reference signal and the error signal may have a phase shift and an amplification with respect to each other. The dynamics of the system to be damped is taken into account by the *filtered x-LMS algorithm.* The update law is then

$$h_i(n+1) = h_i(n) - \alpha e(n)r(n-i), \tag{26}$$

where $r(n - i)$ is the reference signal filtered through the model of the dynamic system between the FIR filter output and the error signal measurement. In other words

[8] Least Mean Squares algorithm.

$$r(n) = G_m(q)x(n)\,, \tag{27}$$

where $G_m(q)$ is the pulse transfer function representing the model of the system. Figure 14 shows a schematic view of the adaptive FIR with the filtered x-LMS algorithm. (Fuller *et al.* 1996, Elliot 2001).

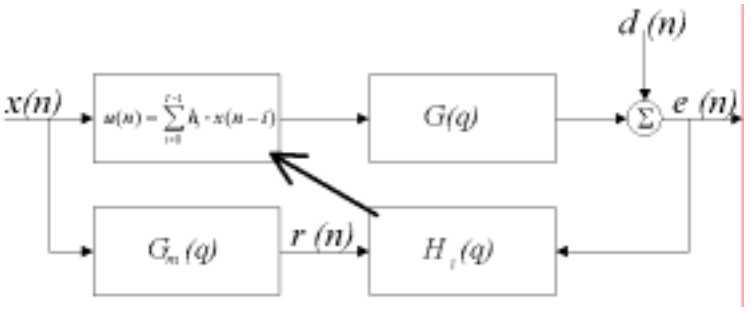

Figure 14. In the filtered x-LMS algorithm, the reference signal is filtered with a system model and used in the coefficient update. The coefficients are then copied into the FIR filter (black arrow).

Several modifications of the LMS algorithm exist. The third update scheme used in this work is the *leaky LMS algorithm*

$$h_i(n+1) = ah_i(n) - \alpha e(n)x(n-i)\,, \tag{28}$$

where *a* is the leakage coefficient, a positive constant less than unity. This feature can be used if the algorithm diverges due to insufficient spectral content (Kataja 1999). By selecting

$$0 < a < 1\,, \tag{29}$$

the integrating action of the update scheme is weakened. The weighting coefficients never achieve the optimal value since they leak away in every update. The performance weakens quickly with the increase of the leaky feature.

The convergence coefficient determines the amount of parameter change in each update. Selection of the convergence coefficient is a trade-off between the convergence rate and stability. The largest stable value for the convergence coefficient is approximately

$$\alpha_{max} \approx \frac{1}{\overline{r^{-2}} I} \tag{30}$$

where α_{max} is the maximum convergence coefficient, $\overline{r^{-2}}$ is the mean square of the reference signal and I is the order of the filter (Fuller *et al.* 1996).

For the filtered x-LMS algorithm and the FIR filter, three signal vectors, each of them equal in length to the order of the filter, have to be stored during control. The first vector is for the weighting coefficients, the second is for the reference signal, and the third is for the filtered reference signal. The operation during one control period can be expressed verbally as follows:

1. Measure the error between the desired value and the actual system output.

2. Measure the reference signal and update the reference signal vector.

3. Filter the reference signal and update the filtered reference signal vector.

4. Compute the weighting coefficients according Equation (26) and update the coefficient vector.

5. Compute the filter output according to Equation (21).

6. Send the output to the force controller.

2.4 Measurements

2.4.1 Experimental set-up

Figure shows the experimental set-up. The measurements of the dynamics of the rotor are reported in Sections 2.4.2 and 2.4.3. The dimensions of the rotor are shown in Figure 16. The actuating forces acted on the armature located at the centre of the shaft. When making measurements for the modal analysis, the displacements were measured at the points marked with black dots, and the excitation induced at the non-drive end of the shaft (+ in Figure 16). When measuring the open-loop behaviour, the displacement was measured at the black dot next to the actuating point. The same point was also used to measure displacement during active vibration control.

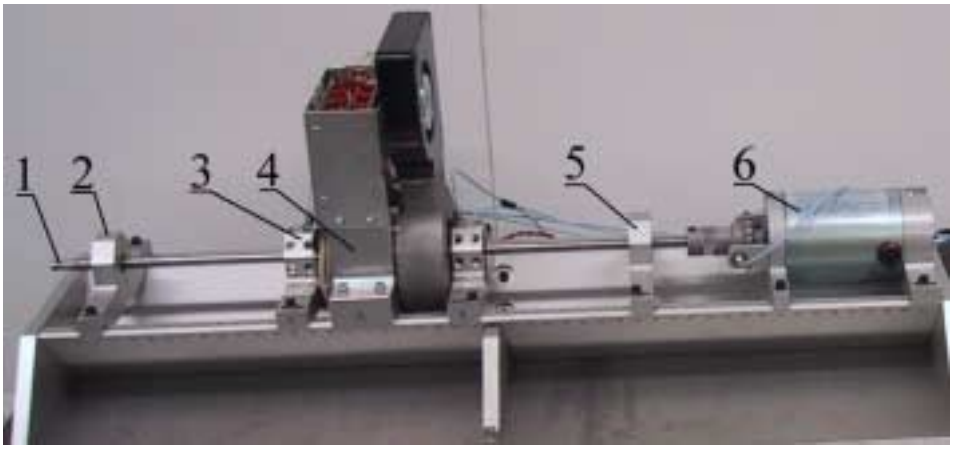

Figure 15. The experimental set-up: 1) rotor, 2) and 5) bearings, 3) displacement transducers, 4) actuator, and 6) driving motor.

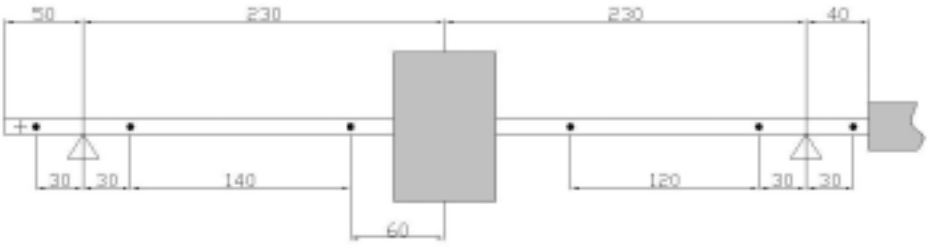

Figure 16. The actuating point is located at the centre of the bearing span. The triangles represent the journal bearings. The armature is located in the middle (shown in grey). The rotor shaft was driven at the right end through the flexible coupling also shown in grey. The displacements were measured at the black dots. The point next to the armature was used in the open-loop measurements and active control.

2.4.2 Modal analysis

The modal analysis was made in order to estimate the modal parameters of the mechanical system and to validate the assumption that the system behaves like a Jeffcott rotor. The measurements were carried out on the non-rotating rotor in the vertical and horizontal planes. The rotor was excited with an impact hammer at the non-drive end (+ in Figure 16). The frequency responses were measured at six points along the rotor with eddy current transducers (black dots in Figure 16). The frequency responses were measured in the direction corresponding to the excitation. The relatively hard head of the impact hammer excited the system up to 400 Hz. The data was analysed on modal analysis software using the SDOF[9] method. The estimated mode shapes are shown in Figure 17. Altogether four natural modes were found in the modal analysis (the two lowest natural modes in the vertical and horizontal planes). The natural frequencies of the first bending modes were about 43 Hz in both planes, the equivalent viscous damping being about 2 %. The natural frequencies of the second bending modes were 296 Hz (horizontal) and 297 Hz (vertical), the damping being about 2 % for both.

[9] Single Degree Of Freedom.

The results correspond to the expectations; the lowest modes have a relatively low frequency while the second modes occur at distinctly higher frequencies.

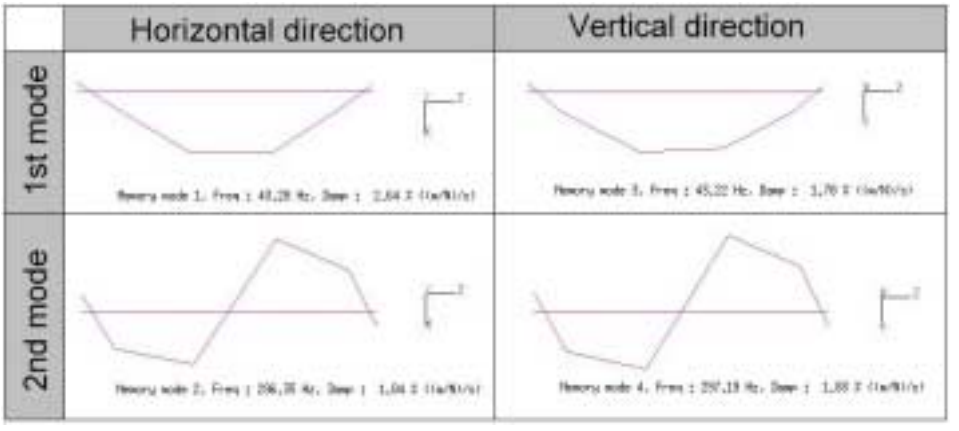

Figure 17. The first two natural modes of the system are shown in the horizontal (X) and vertical (Y) directions (measured on non-rotating shaft).

The results validated the Jeffcott rotor assumption. Naturally, modes at higher frequencies existed. However, the response of the second modes is weak, if excited at the centre of the rotor. This is because the excitation takes place close to the nodal point. The third natural modes do not have a nodal point at the centre of the shaft, but they occur at frequencies higher than those of interest for this work.

2.4.3 Measurements with open-loop system

The open-loop frequency responses were measured in order to identify the mechanical system, the actuator, and the control system together. This was to define the system parameters and again to validate the assumption concerning the Jeffcott rotor. The measurements were carried out by exciting the rotor with the actuator. The force was applied at the middle of the bearing span and the displacement was measured close to the actuating point (see Figure 16). The system was excited separately in the vertical and horizontal directions while the responses were measured in the direction of excitation and in the perpendicular direction. The frequency of the force was swept from 5 Hz to 400 Hz and the

measurements were repeated at several rotational speeds. The control unit had the flux-control loops working during the measurements. The frequency responses with non-rotating shaft in both directions are shown in Figure 18. The magnitude is plotted at the top and the phase at the bottom in the figure. The magnitude showed a sharp resonance at about 40 Hz. The phase also changed quickly in the same region. The second modes were apparent in the phase curve at about 290 Hz. Figure 19 shows the results when run at 1 000 rpm. The amplitude curves in the horizontal and vertical directions were different at the resonance. Elsewhere, they had similar behaviour.

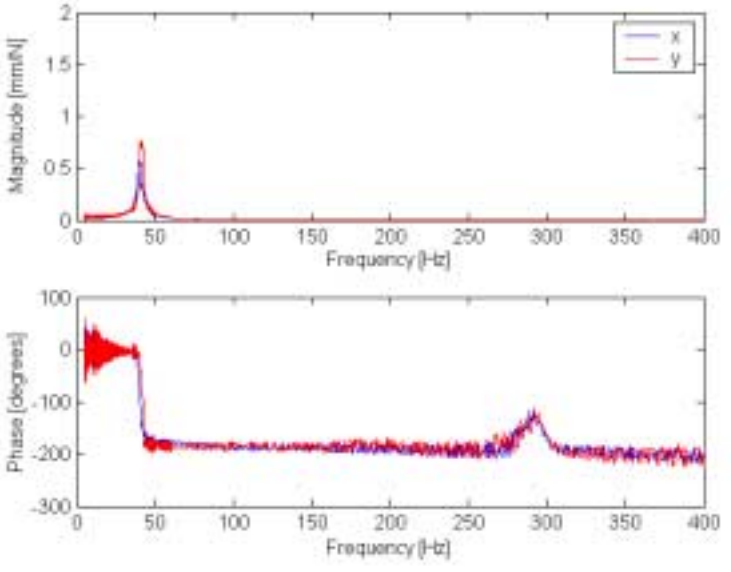

Figure 18. The frequency responses measured for the non-rotating rotor (x: horizontal direction, y: vertical direction). Note that the excitation was reduced at the resonance region in order to avoid the rotor hitting the protective bearing.

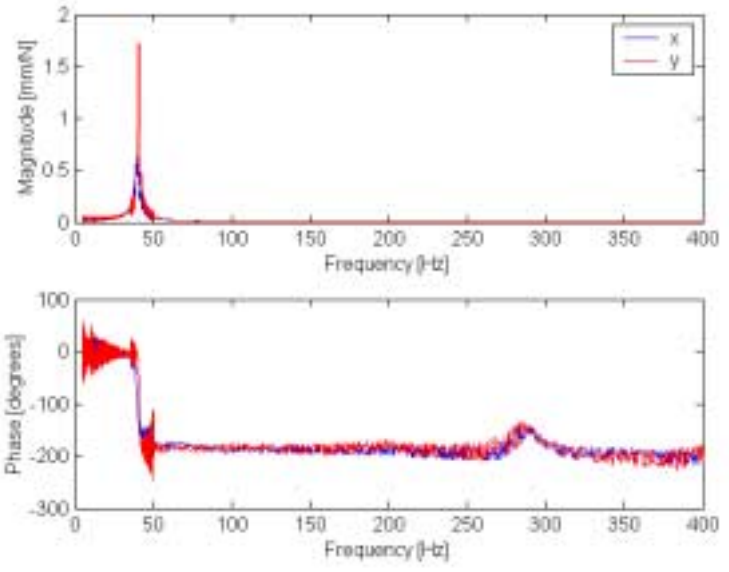

Figure 19. Frequency responses measured with the rotor running at 1 000 rpm.

The measurements showed similar responses for the non-rotating and rotating shaft with the exception of the peak at 40 Hz. The measurements showed that the first natural modes were dominant, as expected. The measurements were also carried out at rotational speeds of 2 000 rpm and 3 000 rpm. They indicated a behaviour similar to the results shown above. The phase curves appear abrupt. In the resonance region, this is due to the manually changed magnitude of the excitation. The magnitude of excitation had to be reduced when the resonance region was approached. Otherwise, the rotor would have hit the safety bearing. Beyond the resonance, the magnitude was increased again in order to excite the system sufficiently and to increase the dynamic range of the displacement transducers. Note that the results of the modal analysis and the open-loop measurements may not be fully comparable, because the excitation methods used were different.

The parameters *m, c* and *k* for the one-degree-of-freedom oscillator model were computed from the parameters achieved in the measurements. The frequency responses were measured from a frequency of 5 Hz upwards. The static gain (the frequency response at 0 Hz) was extrapolated from the measurement results.

The value 0.03 mm/N led to the spring constant k = 33 333 N/m. Measurements indicated natural frequencies of about 40 Hz. The natural frequency in the horizontal direction was slightly lower than in the vertical direction. The equivalent mass m = 0.528 kg was derived by using the natural frequency of 40 Hz. The damping constant was the most difficult parameter to estimate, since measurements indicated different amplitudes at resonance. The amplitude at the resonance was roughly equal to 2 mm/N, which gives the damping constant value c = 2 Ns/m. In Figure 20, all frequency responses are plotted in the same figure, together with the response given by the oscillator model with the values of m, c and k mentioned above.

Generally, a measurement with a swept-frequency sine wave does not always guarantee accurate frequency response functions. On the other hand, a constant sine frequency close to the resonance caused the rotor to hit the safety bearing. The swept frequency was a compromise that made measurement possible near the resonance region. The measurements of the open-loop system indicated a slightly lower first natural frequency than was predicted by the modal analysis. This was probably due to an interaction between the actuator and the mechanical system. It was mainly compensated by the flux-control loop in the control unit but a small effect remained (this negative spring effect is commonly known in electrical machines).

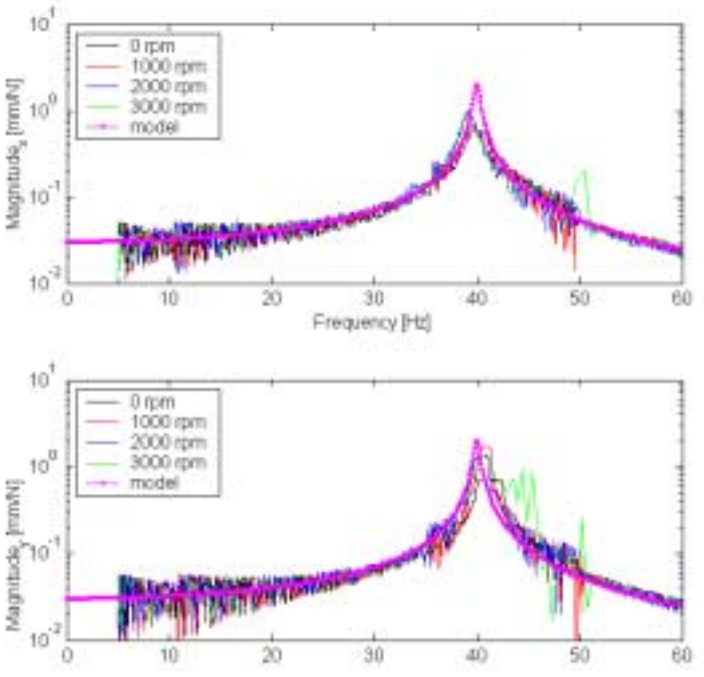

Figure 20. The measurements with different rotational speeds were compared to the model.

The linearity was tested by varying the level of excitation. The frequency responses did not change, *i.e.* the system was considered linear. The parameters computed above were used for the oscillator model in both directions, and no coupling between these two degrees of freedom was assumed. The magnitude of the coupling was measured by computing the frequency response functions from an excitation to the response in the perpendicular direction. Figure 21 shows that the coupling may have had an effect.

On the other hand, it was difficult to estimate the amount of the coupling. The excitation was applied at a relatively high magnitude. For a circular object, a transducer senses the vibration in the transversal direction (Figure 22). Coupling of this kind is strongly dependent on the magnitude of the movement and could be over-estimated in the measurements. For these reasons, the coupling was not taken into account.

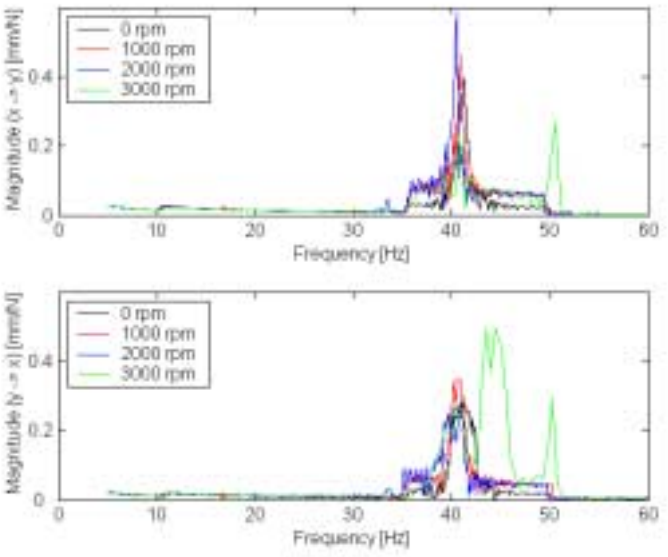

Figure 21. The measurements showed coupling between the horizontal and vertical degrees of freedom. The coupling was to 0.6 mm/N at maximum.

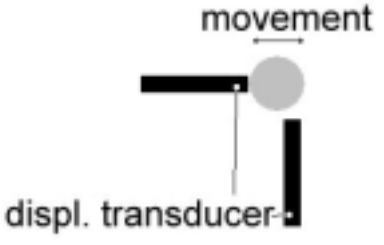

Figure 22. A vertical transducer can sense a horizontal movement owing to the geometry of the measured object.

2.5 Performance & stability

In Section 2.5.1, the feedback control system is analysed by using the parameters obtained in the measurements. The feedforward system is analysed and its implementation in the control unit is discussed in Section 2.5.2.

2.5.1 Feedback control

The measurements provided a sufficient amount of data for defining the parameters of the one-degree-of-freedom oscillator. The open-loop system had poles close to the stability limit at (-1.89 ± i 251) rad/s. The closed-loop poles were placed in the way described earlier. Equation (18) gave a derivative gain of 186 Ns/m, the poles of the closed-loop system being at (-178 ± i 177) rad/s. The measured damping constant was small compared to the derivative gain. Assuming zero damping would not lead to significantly different pole locations; Equation (18) would give a derivative gain of 188 Ns/m. By selecting this figure, the poles of the closed-loop system would actually be located at (-180 ± i 175) rad/s.

A model to simulate the system was built in Matlab Simulink. The model consists of the open-loop system, a disturbance source and the velocity feedback loop. In Figure 23, the difference between the disturbance and the output of the feedback loop is applied to the mechanical oscillator. The velocity feedback loop consists of the zero-order hold (sample-and-hold circuit), derivative computation (the difference of two successive samples divided by the sample time and multiplied by the derivative gain), and the averaging low-pass filter. The sample time used in the simulations was $h = 0.0001$ s, equal to the control period of the control unit.

In order to compare the non-controlled system with the controlled system, simulations were carried out by using a chirp signal as the disturbance. The chirp signal had an amplitude of 1 N, and the frequency increase rate was 0.5 Hz/s. The frequency of excitation increased linearly with the time as it might increase during the run-up of a rotor. In terms of the amplitude, the excitation cannot be considered as a disturbance due to a mass imbalance, because the amplitude is constant over frequency. The responses of the non-controlled and controlled systems are shown in Figure 24. For the non-controlled system, the maximum response was 1.8 mm; it occurred at about 40 Hz. For the controlled system, the maximum response was 0.03 mm around zero frequency. The response of the controlled system did not peak at all at the resonance frequency but decreased with rising frequency.

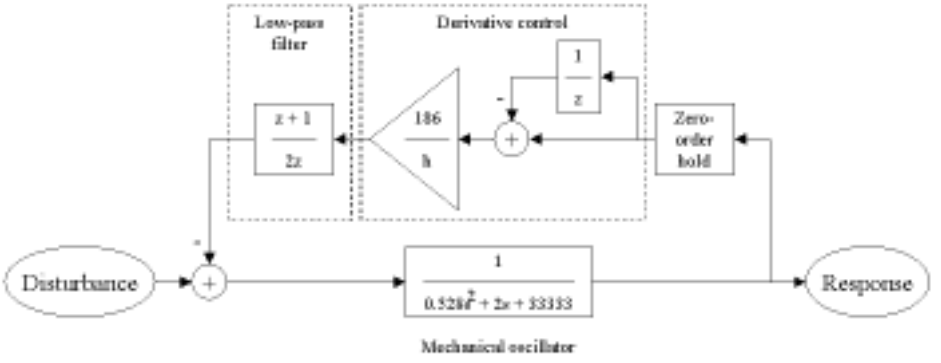

Figure 23. The model included the disturbance and the closed-loop system. The feedback loop consisted of sampling with a zero-order hold, a derivative, and an averaging filter.

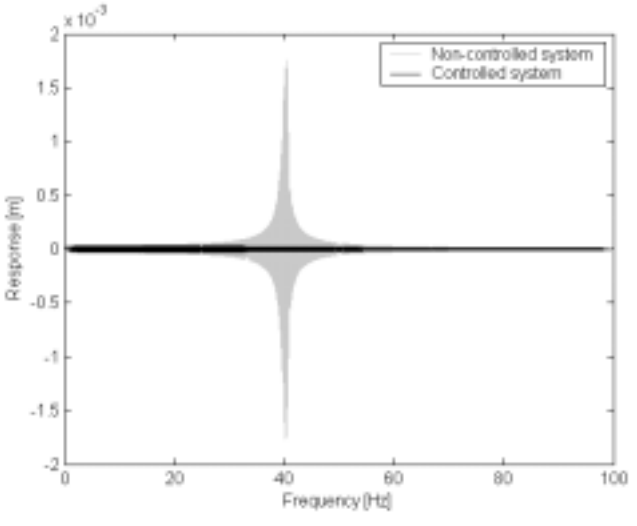

Figure 24. According to the simulations, the response was drastically reduced by active control.

The open-loop system was discretised by the zero-order hold method. Using a 0.0001 s sample time, the open-loop system is described by

$$H_{ol}(z) = 3.0 \cdot 10^{-5} \cdot \frac{0.0003156z + 0.0003156}{z^2 - 1.999z + 0.9996}. \quad (31)$$

With the chosen values of K_d = 186 Ns/m and h = 0.0001 s the transfer function of the feedback compensator is

$$H_{fb}(z) = \frac{186}{0.0001} \frac{(z+1)(z-1)}{2z^2}. \quad (32)$$

The frequency responses of the non-controlled (open-loop) and the controlled (closed-loop) system are shown in Figure 25. The frequency responses were computed from the disturbance to the output. The magnitude curve of the open-loop system has a peak at 40 Hz. The phase of the open-loop system changes rapidly in this resonance region. The closed-loop system does not have any peak at the natural frequency and it has a smoother phase curve than the open-loop system. Hence, the resonance at 40 Hz was effectively damped.

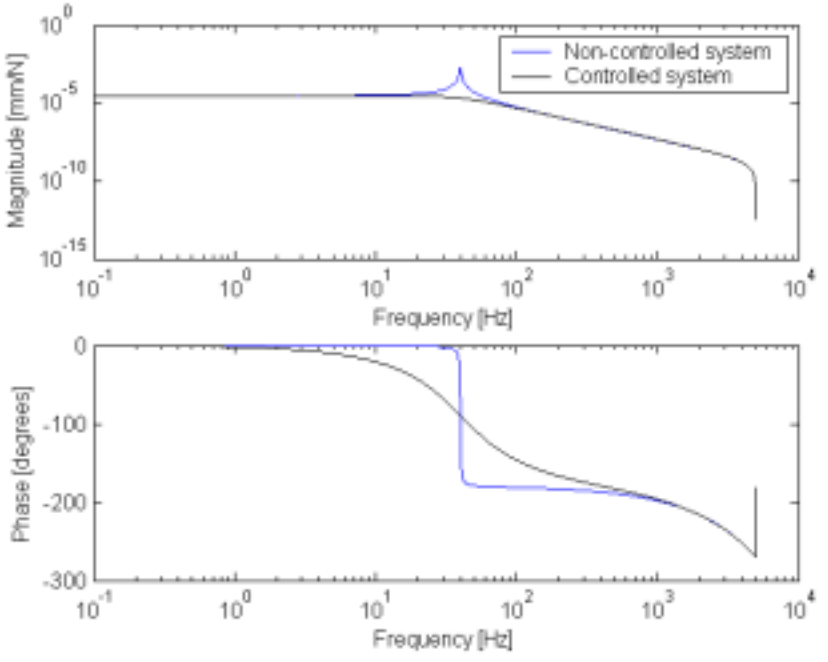

Figure 25. The frequency responses of the non-controlled and the controlled system, computed from the disturbance to the output.

The control unit and the actuator were not modelled for the analysis. They were assumed ideal in these computations. In practice, they form a low-pass filter that restricts the capability of the actuator to produce a force at high frequencies. This may cause stability problems if the mechanical system has a resonance (single or multiple) above the bandwidth of the actuator. In other words, if the Jeffcott rotor assumption is not a sufficiently accurate model, problems may occur.

According to the simulations, the feedback system designed reduced the vibrations in the rotor. Two control systems were implemented in the control unit, one for the vertical direction, and the other for the horizontal direction. No coupling between these was taken into account. The controller can be represented in matrix form:

$$\begin{Bmatrix} F_x \\ F_y \end{Bmatrix} = \begin{bmatrix} H_{fb}(z) & 0 \\ 0 & H_{fb}(z) \end{bmatrix} \begin{Bmatrix} X \\ Y \end{Bmatrix}, \tag{33}$$

where the horizontal control force F_x and the vertical control force F_y are computed from the displacements X and Y in the horizontal and the vertical direction, respectively.

2.5.2 Feedforward control

This section is to discuss the selection of filter parameters and show the results of simulations. The model of the feedforward control system was also built in Matlab Simulink. The simulation model was constructed together with the programming of the algorithm into the control unit because practical considerations set by the control unit had to be taken into account when selecting the filter length and the parameter update frequency. Problems related to the selection of the appropriate order of the filter and the update frequency came up.

The filter of order 2 should theoretically be enough to compensate one frequency. Such a filter would also be persistently excited by one frequency. However, preliminary simulations indicated that the use of an adaptive filter having an order higher than 2 might lead to smoother behaviour. With a filter of order 12, the control unit was able to update the weighting coefficients in one plane during one control period and compute the filter output in the same plane during the next

control period. The update of the weighting coefficients and the output computation in the other plane took another two control periods. It would thus have been possible to run the FIR filter at 2.5 kHz, since control periods in the control unit were performed at a frequency of 10 kHz.

From Equation (1) it is evident that the magnitude of the excitation due to mass imbalance is proportional to the square of the rotational frequency. Hence, compensation of the mass imbalance is less important at low frequencies, say frequencies lower than 20 Hz. It was assumed that the filter should store pulses for at least one half-cycle of the frequency to be compensated. This was explained by the fact that it had to able to compensate an arbitrary phase shift, since the phase relationship of the excitation and the reference signal was not known. The duration of one half-cycle of a 20 Hz signal is equal to 25 ms. A sampling a period of 25 ms by 12 evenly spaced samples leads to an update frequency of 480 Hz. This reasoning gives

$$f_s \approx 2If_c\,, \tag{34}$$

where f_s is the update frequency of the filter, I is the order of the filter, and f_c is the lowest frequency to be compensated. This equation gives an approximation for the filter update frequency. Performing an update in every 20th control period at the control rate of 10 kHz leads to an update frequency of 500 Hz.

In order to estimate the maximum value for the convergence coefficient from Equation (30), the mean square value of the reference signal has to be known. The amplitude of the reference signal generated was scaled to unity. In the case of the LMS algorithm without system model, the maximum allowable convergence coefficient is constant over the frequency band, because the reference signal is used as such. In the case of the filtered x-LMS algorithm, the mean square value of the reference signal is affected by the filtering trough the system model. The system model was scaled in such a way that its static gain was equal to unity. The filtered reference signal also has a maximum amplitude of unity because the feedback-controlled system has its maximum response at zero frequency. This leads to a maximum convergence coefficient of $\alpha_{max} \approx 0.17$. In the simulations, the convergence coefficient was conservatively taken as 0.01.

Figure 26 shows the feedforward compensation and the feedback system together. The reference signal is filtered with a FIR filter and fed into the closed-loop system to compensate the disturbance. The closed-loop system is as described above. The weighting coefficients are estimated according to Equation (25), (26), or (28), depending on the selected parameter update scheme.

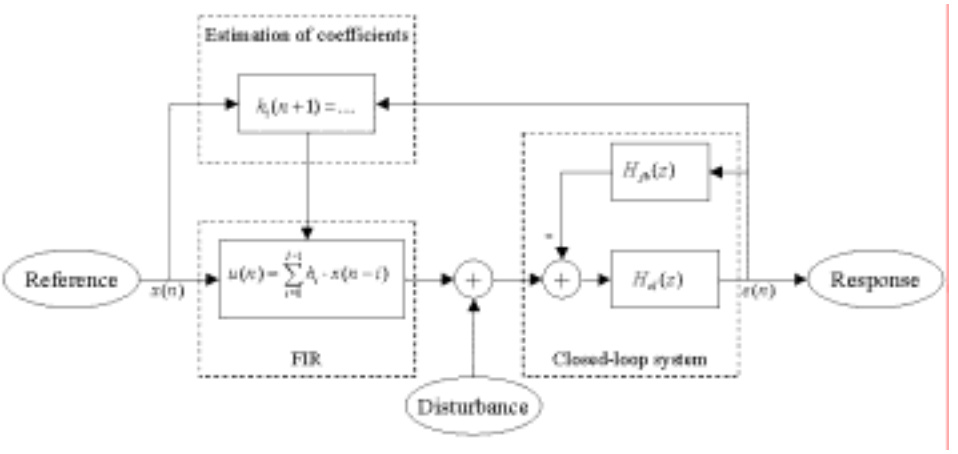

Figure 26. The feedforward control system used in simulations. The block 'Estimation of coefficients' was chosen according to the update schemes in Equations (25), (26), or (28).

First, the simulations were carried out with the update scheme shown in Equation (25). The simulation results with constant frequencies of 10 Hz, 20 Hz, and 30 Hz are shown in Figure 27. The LMS algorithm without the system model converged below the resonance frequency. The rate of convergence became slower when the resonance at 40 Hz was approached. Above the resonance, the algorithm diverged. This behaviour was due to a frequency-dependent phase shift between the reference signal and the output signal of the actual system. According to the literature, the algorithm converges when the phase error is less than 90°. The mathematical interpretation is given as follows by Ren & Kumar (1989)

$$\mathrm{Re}\left[\frac{G_m(e^{i\omega h})}{G_s(e^{i\omega h})}\right] > 0 \quad \forall \quad \omega h, \tag{35}$$

where $G_m(e^{i\omega h})$ is the frequency response of the system model, $G_s(e^{i\omega h})$ is the frequency response of the physical system, ω is the angular frequency, h is the sampling period, and Re represents the operator for taking real part of a complex number. This behaviour was confirmed in the simulations by introducing a varying phase error in the model.

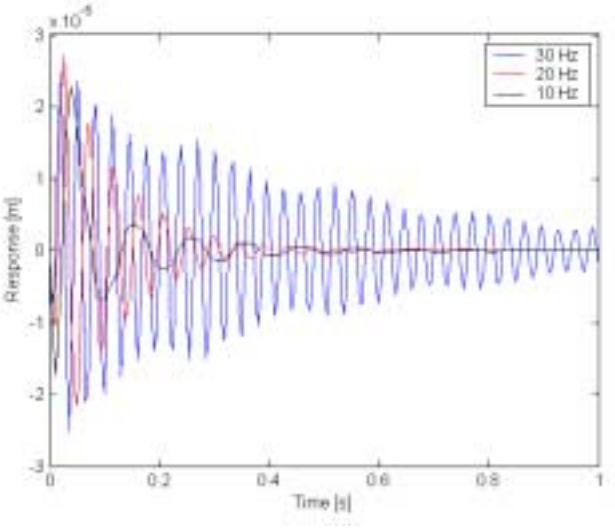

Figure 27. The simulations without system model converged at sub-resonance frequencies. The figure shows responses to unity excitation at frequencies 10 Hz, 20 Hz, and 30 Hz (α = 0.01, I = 12).

Second, the update scheme shown in Equation (26) was implemented by applying the model of the feedback system between the reference signal generation and the parameter update scheme. The system using the filtered x-LMS update scheme was stable also above the resonance frequency. The system model used in the simulations, and to be implemented in the control unit, was

$$G_m(z) = G_{cl}(z), \tag{36}$$

where $G_{cl}(z)$ is the closed-loop pulse transfer function discretised with the zero-order-hold method. Figure 28 shows the response to a sweep from 0 Hz to 100 Hz. The response was largest at low frequencies. This was due to two reasons: Firstly, the adaptation started from zero coefficients with a finite

adaptation speed. Secondly, a filter of 12 coefficients may not form an impulse response accurately enough at low frequencies.

The weighting coefficients of the filter were saved during the simulation. The evolution on the impulse response of the filter was observed from the coefficients. Figure 29 shows the surface plot of the FIR filter coefficients as function of frequency. The evolution was smooth due to the smoothly changing phase curve of the system.

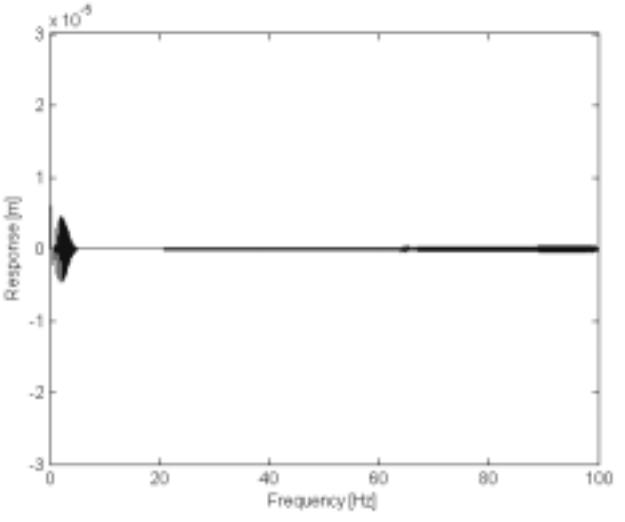

Figure 28. The response during a sweep from 0 Hz to 100 Hz was in the order of micrometres (6 μm at the maximum).

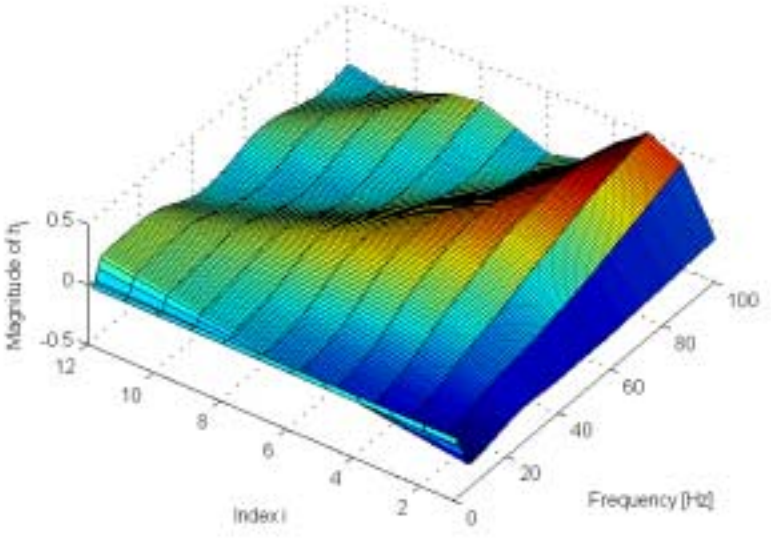

Figure 29. The surface represents the evolution of the filter's impulse response as a function of the exciting frequency. Index 1 refers to the first FIR coefficient (h_0), and Index 12 refers to the last one (h_{11}). The vertical axis represents the magnitude of each coefficient as a function of frequency.

The simulations showed that the LMS algorithm is completely insensitive to the phase shift between the excitation of the system and the input signal of the filter. Thus, a sinusoidal signal generated from rotational pulses could be used as a filter input signal.

In terms of input-output stability, a FIR filter always gives a bounded output signal for a bounded input signal. The magnitude of the output signal can be restricted to an arbitrary value by limiting the absolute value of the coefficients h_i. The convergence of the LMS algorithm itself can be guaranteed by choosing an appropriate convergence coefficient α. However, even if the convergence coefficient α is appropriately chosen, the algorithm can end up amplifying vibrations due to a phase error caused by an inaccurate system model. As mentioned before, this phase error should not be larger than 90°. The requirements for the quality of the system model were formulated in Equation (35).

The selection of the convergence coefficient is a trade-off between the speed of adaptation and possible divergence of the algorithm. The maximum value for the convergence coefficient α given in Equation (30) is not an exact limit. Note also that the convergence of the filtered x-LMS algorithm is frequency-dependent because the amplitude of the filtered reference signal is frequency-dependent.

3. Results

The control systems discussed were programmed into the control unit and tested in the test environment. The results with feedback control only are shown in Section 3.1. Section 3.2 presents the results obtained when both algorithms, feedback and feedforward control, were functioning, but the model of the system was not used by the adaptive algorithm. The results shown in Section 3.3 were obtained when the system model was added to the adaptive algorithm. In Section 3.4, a comparison of the control forces used in the different cases is shown.

In order to facilitate the interpretation of results, a relative measure for the rotational speed was utilised. The relative speed of the rotor is the ratio between the rotational speed and the critical speed

$$r = \frac{\omega}{\omega_{cr}}, \tag{37}$$

where ω is the rotational speed in radians per second.

3.1 Feedback control

Figure 30 shows the displacement signals measured in a run-up condition. The run-up was performed from 4.2 Hz ($r = 0.1$) to 65 Hz ($r = 1.6$) at a rate of 16.7 Hz/min (1 000 rpm/min). Active control was switched on at 38 Hz, just before crossing the critical speed. The control was switched off at 52 Hz. At the beginning of the run-up, at rotational speeds lower than 20 Hz, the response was about 20 microns (peak). From 20 Hz to the switch-on point of the active control, vibrations increased, reaching 180 microns. Active control reduced the response to about 20 microns until it increased to about 50 microns at the switch-off point of the active control. Note that a multiple of the rotational frequency also excited the resonance frequency, as can be seen clearly from the vertical response at 20 Hz in Figure 30. The peak at 20 Hz indicated that the test rotor did not exactly behave like the Jeffcott rotor, because the Jeffcott rotor is excited only at the frequency of rotation.

Another run-up was performed, from 4.2 Hz ($r = 0.1$) to 83.3 Hz ($r = 2.1$) with active control constantly on (Figure 31). The behaviour was smooth; the amplitude of the response did not exceed 22 microns (peak) at any speed.

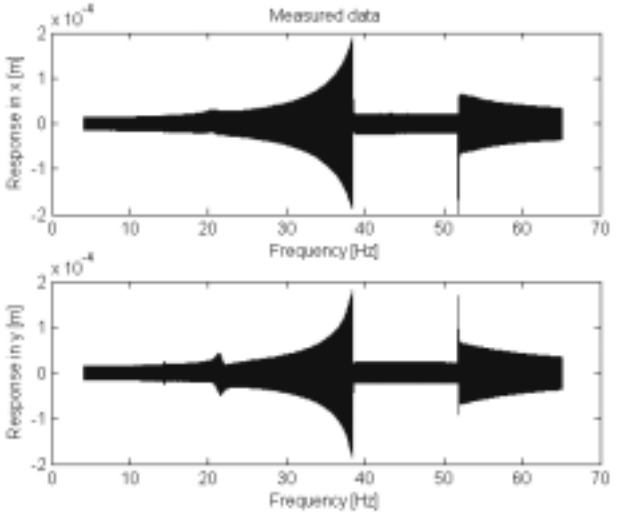

Figure 30. The measured response shown as a function of the rotational frequency. The vibration in the horizontal direction (top) and the vertical direction (bottom) were reduced significantly when control was switched on before crossing the critical speed.

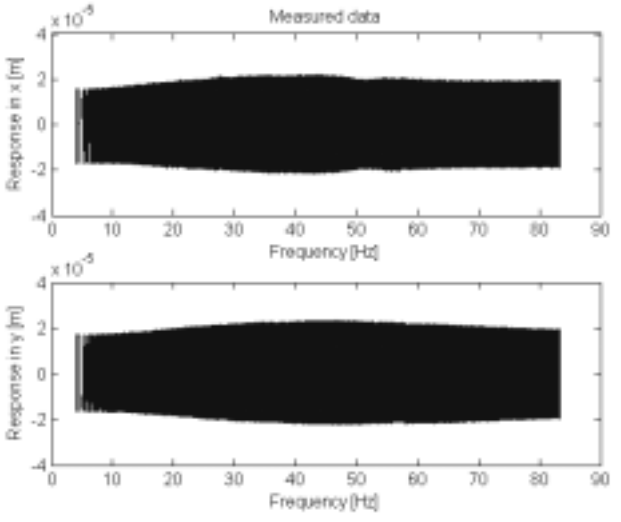

Figure 31. Run-up with active control on from 4.2 Hz (250 rpm) to 83.3 Hz (5 000 rpm). The active control restricted the vibration amplitude effectively during run-up. Note the different scales used in Figure 30 and Figure 31.

The orbit of one point in the rotor was measured at 36.7 Hz (r = 0.9, Figure 32). The same transducers were used for the measurement and for the inputs to active control. The controlled rotor had an orbit diameter of about 50 microns, while the orbit diameter without control was about 260 microns. The orbit of the controlled rotor was found slightly more circular but slightly cornered compared to the orbit of the freely running rotor, which was elliptical.

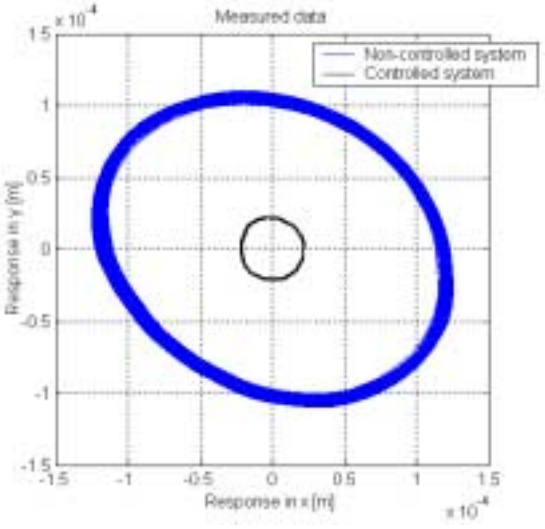

Figure 32. Orbits measured when running at 36.7 Hz (2 200 rpm), with and without the active control.

The controlled and the non-controlled systems were compared in the frequency domain (Figure 33). The spectra were computed from displacement signals recorded when the rotor was running at 36.7 Hz (autopower spectrum, flattop window, 0.5 Hz frequency resolution, 75 % overlap, 125 averages). In the frequency band from 30 Hz to 50 Hz, the response with the active control on was approximately one tenth of the response in the non-controlled case.

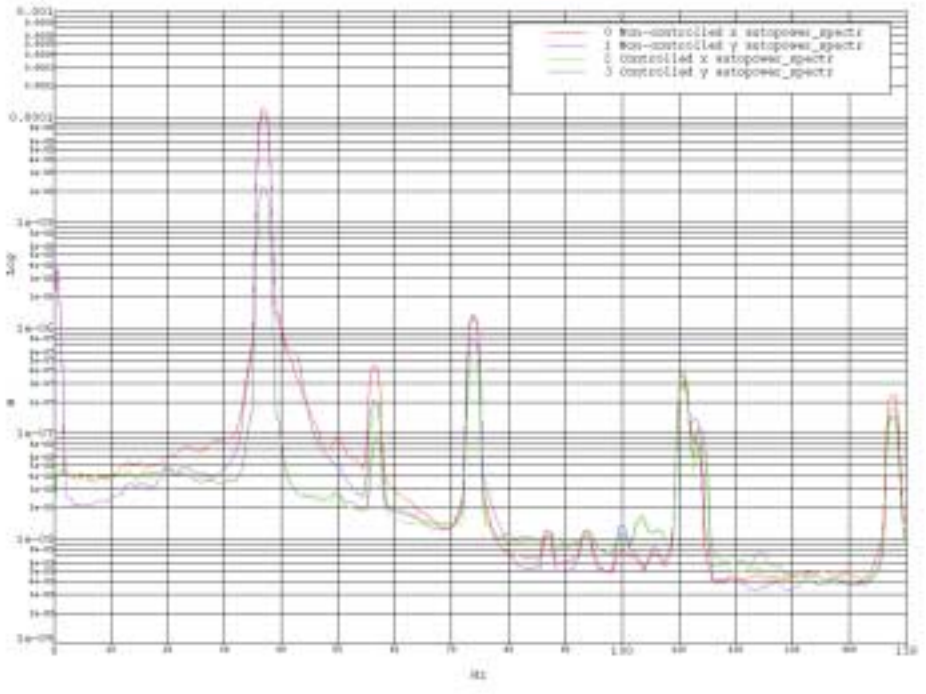

Figure 33. Feedback control reduced the response at the rotational speed and in the resonance region. The curves '0 Non-controlled x' and '1 Non-controlled y' were measured in the non-controlled case in the X and Y planes, respectively. The curves '2 Controlled x' and '3 Controlled y' were measured with feedback control active.

3.2 Feedforward control without system model

The adaptive filter not using the system model was tested first (*i.e.* update scheme in Equation (25)). The tests were carried out from 11 Hz upwards. The lowest frequency was dictated by the characteristics of the rotational speed sensor, which worked at frequencies above 10 Hz. The response during the switch-on period of the filter is shown in Figure 34. The response rose slightly right after switch-on, but it began to decrease in about half a second. During the next 10 seconds, the response was diminished from 20 microns to 2 microns. The rotational speed was 31.7 Hz (r = 0.8) and the convergence coefficient was 0.01.

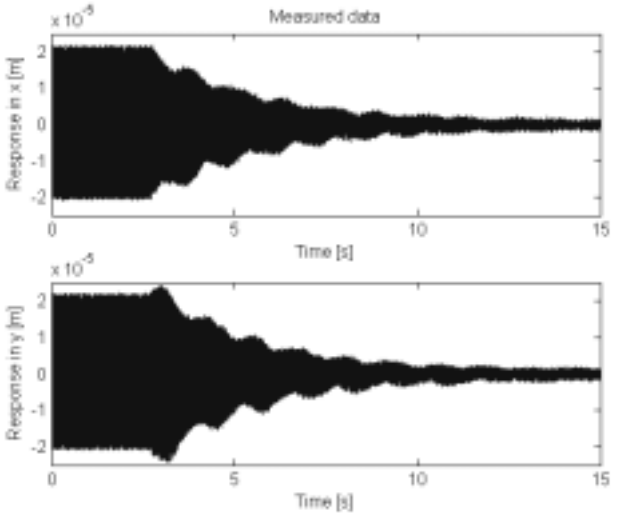

Figure 34. The responses in the X (top) and the Y direction (bottom) were measured during a FIR filter switch-on sequence. The feedback control was running alone at the beginning of the time record. Then, the adaptive FIR filter was switched on. The system converged, reaching the steady-state condition in about 10 seconds.

At almost all frequencies in the sub-critical range, the response was reduced compared to the response using the feedback control alone. However, approaching the critical speed was found problematic. At rotational frequencies over 34 Hz, the algorithm diverged and amplified the vibrations. This behaviour, estimated in the simulations, was due to a frequency-dependent phase shift between the reference and the response. The algorithm was tested with different convergence coefficients; these seemed not to affect the problem. However, the coefficient had a significant effect on the speed of convergence, or the speed of divergence. The effects of the leaky update scheme, in Equation (28), were studied. The algorithm did not diverge if the leaky constant was chosen as slightly less than unity, for example $a = 0.99$. However, the performance of the algorithm was quickly ruined.

Analysis in the frequency domain showed that the harmonic vibration induced by mass imbalance was almost completely compensated (Figure 35). The displacement spectra were computed from time signals recorded when running at

31.7 Hz (1 900 rpm) without control, with the feedback control only, and with both control algorithms together (autopower spectrum, flattop window, 0.5 Hz frequency resolution, 75 % overlap, 125 averages). Comparison between the non-controlled and the controlled cases showed that the first harmonic was attenuated mainly by virtue of the feedforward control. Contrary to this, the vibration at the natural frequency was damped by the feedback control. Active control had a slight damping effect on the remaining higher harmonics. A similar behaviour was measured in the vertical direction (Figure 36).

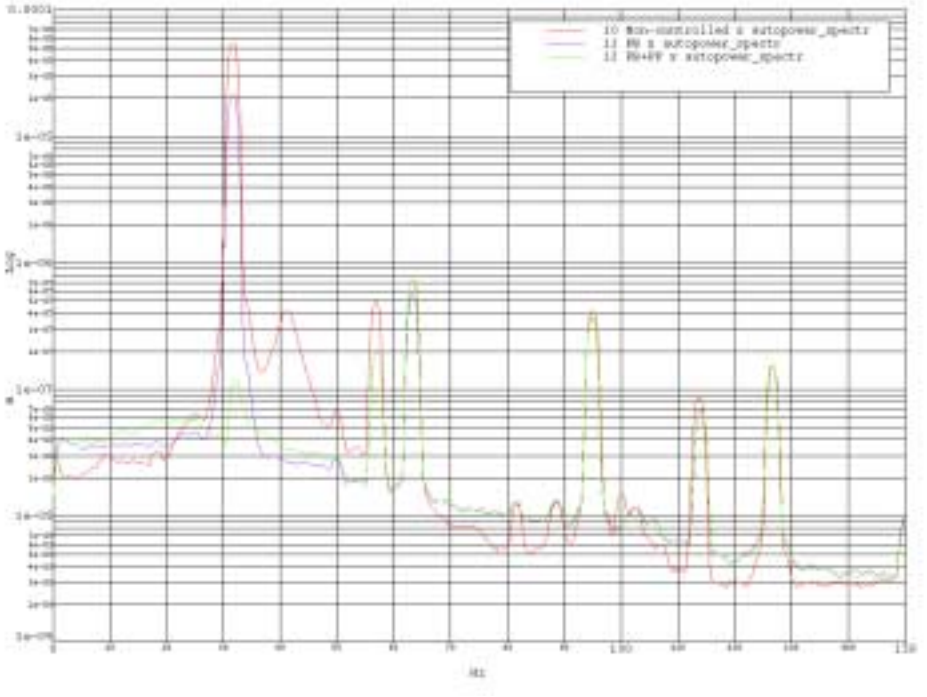

Figure 35. The displacement spectra shown in the X-direction, without control (curve '10 Non-controlled x'), feedback control on (curve '11 FB x') and both algorithms working (curve '12 FB+FF x').

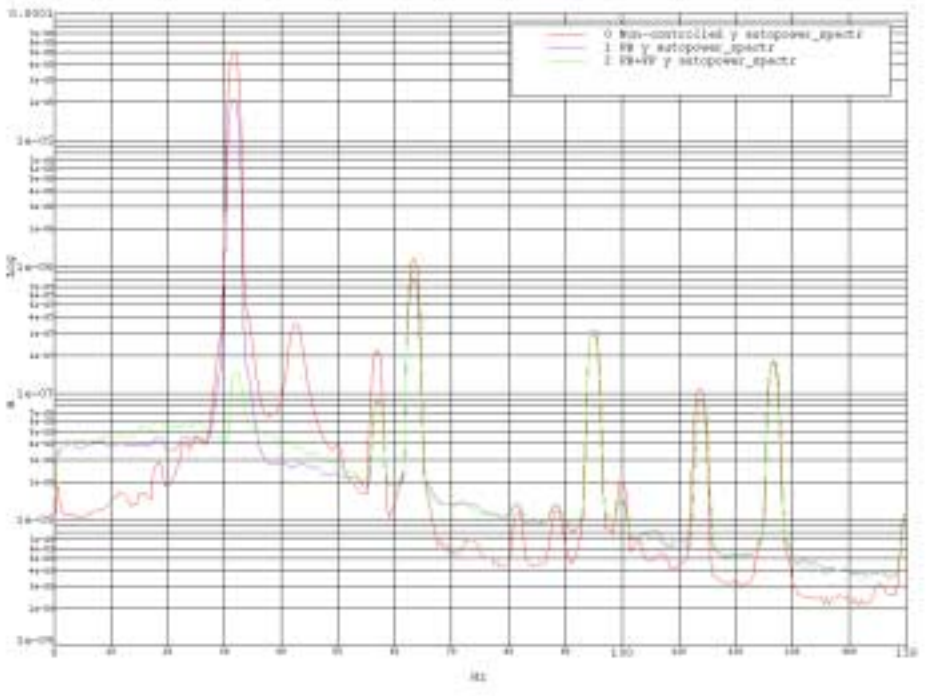

Figure 36. The displacement spectra shown in the Y-direction, without control (curve '0 Non-controlled y'), feedback control on (curve '1 FB y') and both algorithms working (curve '2 FB+FF y').

3.3 Feedforward control with system model

The tests were also carried out with the adaptive x-LMS algorithm running. The convergence coefficient used in the tests was 0.01. At sub-critical speeds, the algorithm with the system model converged faster than the algorithm without the system model. Figure 37 shows the response when the feedforward compensation was switched on at 31.7 Hz (compare with Figure 34). The algorithm converged in about one and a half second. The algorithm also showed stable behaviour at super-critical speeds; Figure 38 shows the response during a switch-on period when running at the critical speed. The convergence took about one and a half second at super-critical speeds. In both plots, the convergence was continuous. The fluctuation observed in the convergence in the case without system model was absent. This can also be seen from the orbit of the rotor, measured by the same transducers as the active control system used (Figure 39).

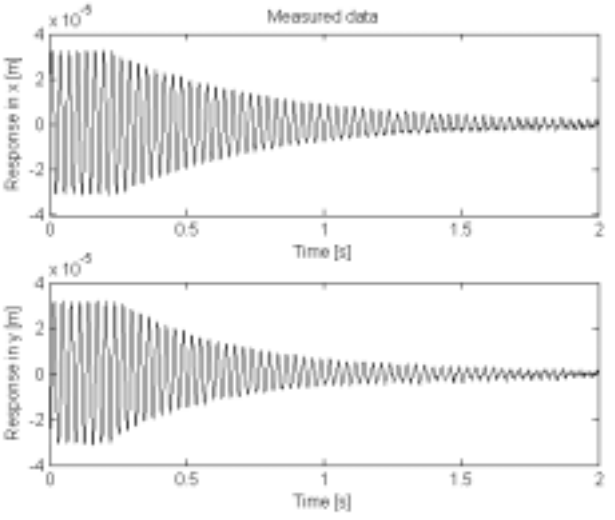

Figure 37. The adaptive FIR filter with system model was switched on when running at 31.7 Hz (r = 0.8). The system converged, reaching the steady-state condition in about 1.5 s.

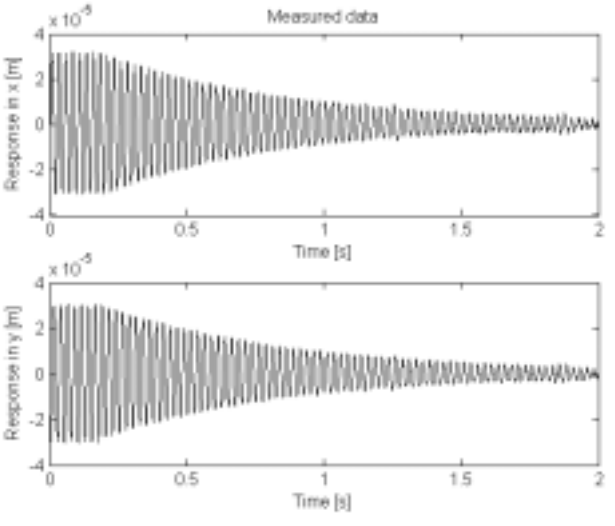

Figure 38. The adaptive FIR filter with system model was switched on when running at 40 Hz (r = 1.0). The system converged, reaching the steady-state condition in about 1.5 s.

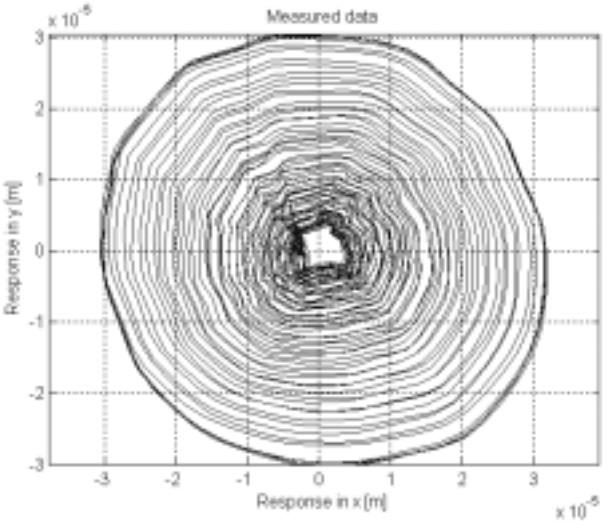

Figure 39. The orbit of the rotor during switch-on of the adaptive filter indicated smooth convergence, the rotational speed being 40 Hz. A time span of 1.46 seconds is shown in the orbit plot.

Figure 40 shows the responses in the horizontal and vertical directions during a sweep from 11 Hz to 65 Hz. The response diminished from 5 microns to 2 microns as the rotational speed increased from 11 Hz to 18 Hz. From 18 Hz to 45 Hz (r = 0.45−1.1), the response was approximately constant, being about 2 microns. Above 45 Hz, higher peaks in the response occurred randomly. The highest peak observed was 42 microns in the vertical direction. Correlation with the quality of the reference signal was observed. The reference signal had a discontinuity at the instant when the peak occurred.

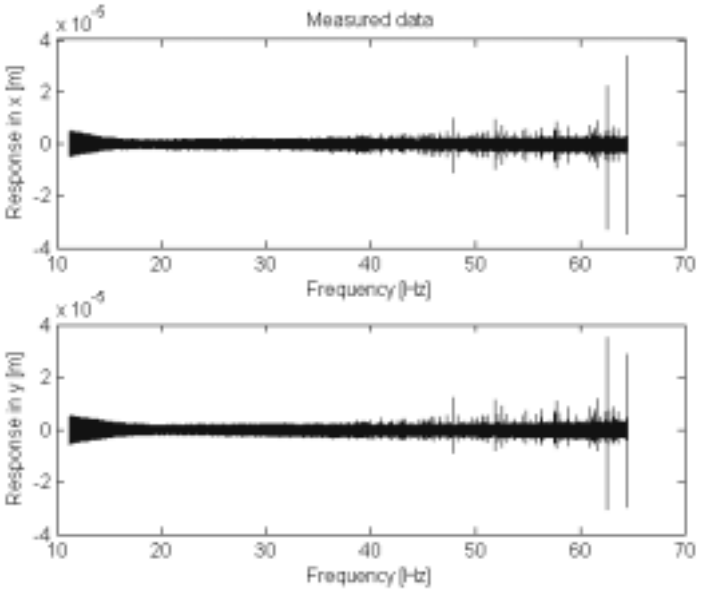

Figure 40. Responses measured when the rotational speed was swept from 11 Hz to 65 Hz.

3.4 On the forces used in active control

The control commands computed in the control algorithms were compared in order to study the characteristics of the algorithms, and to estimate the force required for the control. The feedforward algorithm used was the x-LMS algorithm. When the adaptive filter was switched off, the total control force was equal to the force computed by the feedback loop. When the adaptive filter was switched on, the total force was the resultant of the forces computed in the feedback loop and the feedforward loop.

The control commands produced by the feedback control and by the feedforward control were recorded separately. Figure 41 shows the control command as a function of time when the rotational speed was 25 Hz ($r = 0.6$). The control commands computed in the feedback loop were characterised by one sinusoid at 25 Hz when the feedforward compensation was off. The control commands of the feedback loop were reduced when the feedforward compensation was switched

on. This was because the 25 Hz sinusoid was now compensated by the feedforward loop.

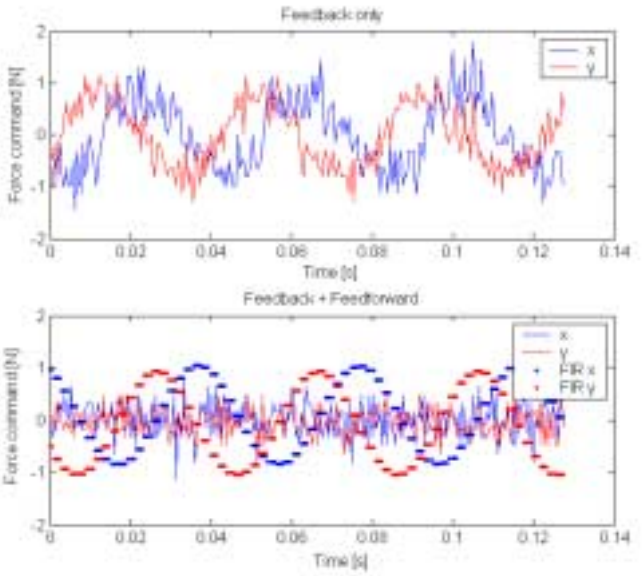

Figure 41. The commands for the control forces recorded when using the feedback control only (top) and both control algorithms (bottom). The rotational speed was 25 Hz. The phase between the subplots should not be compared, since the measurements were not synchronously triggered.

Figure 42 shows the corresponding behaviour in super-critical operating conditions at a rotational speed of 65 Hz (r = 1.6). The force commands from the feedforward compensation were rather edgy at 65 Hz, since the update frequency of the FIR filter output was 500 Hz. The magnitude of the sinusoidal feedforward compensation force was roughly doubled when the rotational speed was increased from 25 Hz to 65 Hz. The root-mean-square (rms) values of the control force commands were computed at rotational speeds of 25 Hz, 40 Hz, and 65 Hz. Table 2 shows the rms values of the control force commands at three rotational speeds. In the case of feedback control only, the magnitude of the feedback force was from 0.9 N to 2.1 N. When using feedforward control, the magnitude of the feedback force was reduced to about half.

It is important to notice that the total control force was not increased when using the feedforward compensation even when the response was substantially reduced. Hence, the control force was used in a more effective way by the feedforward system. Note also that the force commands were not proportional to the square of the rotational speed. Rather, they were linearly proportional to the rotational speed.

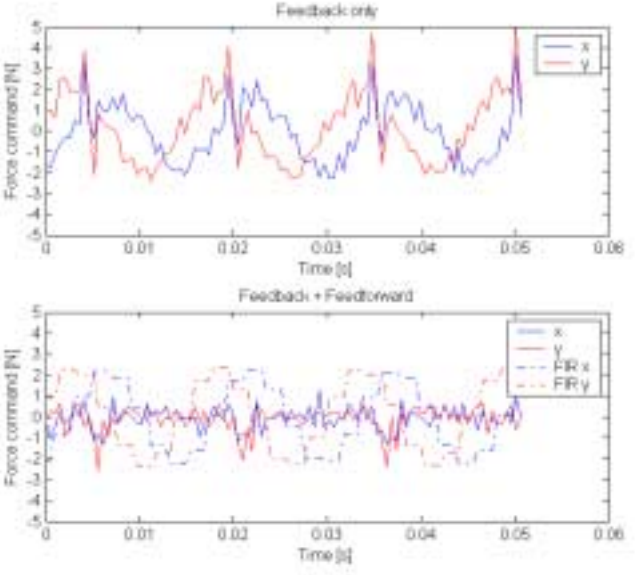

Figure 42. The commands when using the feedback control only (top) and both control algorithms (bottom). The rotational speed was 65 Hz

Table 2. The control force commands computed by the feedback (FB) and the feedforward (FF) control algorithms at three rotational speeds (rms values).

Rotational speed		FB control only		FB + FF control together			
		FB force	Displacement	FB force	FF force	FB+FF	Displacement
[Hz]	[rpm]	[N]	[microns]	[N]	[N]	[N]	[microns]
25	1500	**0.9**	26.2	**0.4**	**1.0**	**1.1**	1.2
40	2400	**1.4**	27.6	**0.6**	**1.3**	**1.4**	1.1
65	3900	**2.1**	24.1	**0.9**	**2.3**	**2.5**	1.5

4. Discussion

Vibrations around the critical speed were efficiently damped by velocity feedback control. It provided a possibility to run the rotor at critical speed by virtue of increased damping. It also provided smoother phase characteristics, which made feedforward compensation easier.

The velocity feedback is a textbook example for active vibration control in general (Ylén & Virkkunen 1995, Preumont 2002). One reason for this is the characteristically low damping of mechanical systems; a significant reduction in response can be achieved by a simple controller acting against vibration velocity. Another reason is that the stability of the collocated system can be guaranteed for an ideal control system (Preumont 2002). According to the literature review, the control method has also been applied to rotors. The present study supports the use of velocity feedback for active vibration control of rotors. This study also shows that the reduction is significant in the resonance region for a rotor with low external damping.

The resonance can also be shifted with the control system by implementing a control force proportional to the displacement of the rotor. A load-carrying function is thus applied. This was briefly tested and found to work in the test environment. However, this was out of focus, because very large forces would be required in heavy rotating machines.

For the present study, feedforward compensation without a system model worked according to the predictions: the algorithm converged at low frequencies, but diverged when the resonance was approached. It was noticed that the leaky feature in the algorithm extended the usable frequency range, but reduced the performance. Feedforward compensation with the system model converged also during super-critical operation. However, higher peaks occurred randomly at rotational speeds above 45 Hz. The reason for this behaviour was not completely clear; it can be due to poor quality of the reference signal, an inappropriate choice of filter parameters, or rotordynamic phenomena. The first, and the most probable, reason were discontinuities occurring in the reference signal simultaneously with the peaks in the response. It was difficult to determine which of them was the reason and which was the cause. Second, the length and the update frequency of the filter were selected in such a way that the compensating

signal was coarse at high frequencies. This probably produced high frequency components, which excited the rotor. Third, the explanation involving rotordynamic phenomena is based on the fact that a super-critical rotor rotates around its centre of gravity, while the compensation was forcing the rotor to rotate around its geometrical centre.

Several feedforward compensation algorithms have been studied for synchronous force cancellation in active magnetic bearing applications (Knospe *et al.* 1997, Lantto 1999). Adaptive finite-impulse-response filters and the least-mean-squares algorithms have been used in noise and vibration control (Fuller *et al.* 1996, Elliot 2001). The present study proposes a novel application area for adaptive finite-impulse-response filters. The use of a reference signal is one common feature in these applications, but the adaptation mechanisms differ. The study confirms that remarkable reductions in response can be achieved by compensating the disturbance by means of a reference signal.

The different roles of the algorithms were pointed out. Feedback control added viscous-like damping to the system and provided a system with smooth response for feedforward compensation. Feedforward control compensated the largest source of excitation, which occurred at the rotational speed. The comparison between the forces computed by the different control algorithms showed that the magnitude of the force did not increase although the response was significantly reduced when feedforward control was applied. The magnitude of the control forces used was only from 1 N to 3 N (according to the control commands) which is low compared to the mass of the rotor (1.1 kg). Thus, a significant reduction in response can be achieved with a low actively controlled force. This fact was also shown by the example in Section 2.2.

The test environment chosen was suitable for the purpose in terms of flexibility and functionality. The rotor kit was easy to modify and good for demonstration purposes. The control unit was found to be a flexible and robust device with a well-organised user interface. It turned out that heat dissipation should be considered when designing an actuator. The total air gap dictates the maximum force available. If the actuator is required to produce very large forces, the Hall transducers cannot be placed in the air gap in the way they were in the present design. On the other hand, the air gap will not grow in proportion to the scale, and

the current density will decrease with the scale. Thus, the situation could be easier with a larger rotor diameter.

The adaptive filter indicated a few challenges that may occur when implementing an adaptive controller in a full-scale system of this kind. Firstly, testing was difficult, the code had to be correctly programmed, and the algorithm had to work properly before switching the magnetic actuator on. Secondly, testing the adaptive properties was impossible unless the actuator was active, because the adaptation had no feedback from the parameter changes it performed. Thirdly, the adaptive algorithm had to be switched off when not running in its operating range *e.g.* when no reference signal was available. Fourthly, correct operation had to be monitored manually and required human judgement. These challenges can all be solved, but they require some attention, maybe more than the control algorithms used.

4.1 Future work

The test set-up used was simplified: one vibration mode in each direction, no gyroscopic effects, actuator in the middle, excitation due to imbalance *etc*. Such complications as several natural modes, a non-symmetrically located actuator, and excitation from the foundation occur in 'real' machines. They place additional demands on control system design, and they should be studied in the future. Furthermore, the scale of the test environment is modest. This fact should to be discussed and solved by first using a larger-scale model and then moving on to a larger-scale test environment.

The performance of the adaptive filter was affected by the selection of the filter parameters and their update frequency. These effects should be studied deeper and rules should be set for the design. Other algorithms for the purpose should also be studied. The algorithm called convergent control was designed for the feedforward compensation as was the adaptive FIR. These two algorithms should be compared in terms of performance, stability, and computational power required.

The control system design was based on knowledge available about the system to be controlled, and the parameters were assumed invariant in time. The goal for

future work is automatic system identification, preferably integrated into the control system. Adaptive control and system identification methods should be studied to achieve the goal. Furthermore, the question of the necessary minimum of knowledge about the system should be addressed in order to avoid excessively complicated adaptive designs.

5. Summary

The test rotor test environment comprised the rotor kit, the magnetic actuator and the control unit. The set-up used was designed to imitate the Jeffcott rotor. The measurements confirmed that the system approximately behaved as a Jeffcott rotor having a sharp resonance at 40 Hz. Without any control system, running close to the critical speed was not possible without the rotor touching the protective bearing.

Active vibration control systems were designed by using parameters determined through measurements. The velocity feedback control was designed to move the closed-loop poles further away from the stability limit. The feedback control reduced the vibrations remarkably in the vicinity of the critical speed and provided approximately constant response at rotational speeds from 4 Hz to 83 Hz.

A feedforward system was applied for the compensation of a mass imbalance in the rotor. The feedforward compensation consisted of an adaptive finite-impulse-response filter adapted with the least-mean-square algorithm. A sinusoidal signal generated from rotational pulses was used as a reference signal for the filter. The feedforward system reduced the response to about one tenth compared to the response with velocity feedback alone. The use of the system model in the algorithm extended the operating range beyond the critical speed of the rotor.

For example, when running at 1 900 rpm (the relative speed $r = 0.8$), the response without any control was about 60 microns (peak). The response was lowered to around 20−30 microns by the velocity feedback. When added to the velocity feedback, the adaptive FIR filter reduced the response to the order of 2 microns. The active forces required for the control, from 1 N to 3 N, were low compared to the mass of the rotor (about 1.1 kg).

References

Cheung L.Y., Dunn R.W. & Daniels A.R. & Berry T. *Active vibration control of rotor systems*. Control '94. IEEE. 1994. Pp. 1157–1163.

Ehmann, C., Alizadeh, A. & Nordmann, R. *Schwingungsdämpfung aktiv gelagerter Rotoren mit robuster Regelung, in Schwingungen in rotierenden Maschinen.* Feb. 2003, Darmstadt.

Elliot S.J. *Signal processing for active control*. Academic Press. London. 2001. 511 p. ISBN 0-12-237085-6.

Fuller C.R., Elliot S.J. & Nelson P.A. *Active control of vibration*. Academic Press. London. 1996. 332 p. ISBN 0-12-269440-6.

Gasch R., Nordmann R. & Pfutzner H. *Rotordynamik*. Springer-Verlag. Berlin. 2002. 705 p. ISBN 3-540-41240-9.

Genta G. *Vibration of structures and machines*. Springer-Verlag. New York. 1999. 591 p. ISBN 0-387-98506-9.

Glad T. & Ljung L. *Control theory*. Taylor & Francis. London. 2000. 467 p. ISBN 0-7484-0878-9.

Ioannou P.A. & Sun J. *Robust adaptive control*. Prentice-Hall, Inc. USA. 1996. 825 p. ISBN 0-13-439100-4.

Ishimatsu T., Shimomachi T. & Taguchi N. *Active vibration control of flexible rotor using electromagnetic damper*. International Conference on Industrial Eletronics, Control and Instrumentation. IEEE. 1991. Pp 437-441.

Järviluoma M. & Valkonen A. *Test equipment and controller for active rotor vibration damping*. Progress report. VTT Automation. Oulu. 2001. 38 p.

Järviluoma M. & Valkonen A. *Test equipment and controller for active rotor vibration damping: set-up, methods, results*. Progress report. VTT Automation. Oulu. 2002. 53 p.

Kataja J. *Applications of adaptive algorithms for active noise control*. Tampere University of Technology. 1999. 99 p. Master's thesis.

Knopf E. & Nordmann R. *Active magnetic bearings for the accurate force measurement in rotating machinery*. The Fourth International Conference on Motion and Vibration Control. ETH Zurich. 1998.

Knospe C.R., Fedigan S.J., Hope R.W. & Williams R.D. *A multitasking DSP implementation of adaptive magnetic bearing control*. Transactions on Control Systems Technology, 1997, Vol 5, No 2, pp 230–238.

Krämer E. *Dynamics of rotors and foundations*. Springer-Verlag. Germany. 1993. 383 p. ISBN 3-540-55725-3.

Lantto E. *Robust control of magnetic bearings in subcritical machines*. Acta Polytechnica Scandinavica. The Finnish Academy of Technology. Espoo. 1999. 143 p. Doctoral dissertation. ISBN 592-5148-80-7.

Preumont A. *Vibration control of active structures*. Kluwer Academic Publishers. Netherlands. 2002. 364 p. ISBN 1-4020-0925-9.

Ren W. & Kumar P.R. *Adaptive active noise control: structures, algorithms and convergence analysis*. Proceedings of Inter-Noise 89. Vol 1. 1989. Pp. 435–440.

Schweitzer G., Bleurer H. & Traxler A. *Active magnetic bearings*. Hochschulverlag AG. ETH Zurich. 1994. 244 p. ISBN 3-7281-2132-0.

Sun J.C., Wang X.G. & Xi F.J. *Sliding mode active vibration control of circular saws*. International Conference on Control Applications. IEEE. 2000. pp 953–958.

Sun L., Krodkiewski J.M. & Cen Y. *Self-tuning adaptive control of forced vibration in rotor systems using an active journal bearing*. Journal of Sound and Vibration, 1998, Vol 213, No 1, pp 1–14.

Vance J.M. *Rotordynamics of turbomachinery*. John Wiley & Sons, Inc. USA. 1987. 388 p. ISBN 0-471-80258-1.

Wang J. & Meng G. *Instability of a cantilever rotor supported on MR fluid damper and sliding bearing*. Sixth International Conference on Rotor Dynamics. Vol 2. IFToMM. Sydney. 2002. Pp 615–620. ISBN 0-7334-1962-3.

Ylén J-P. & Virkkunen J. *Säätötekniikan harjoitustehtäviä*. Hakapaino Oy. Helsinki. 1995. 252 p. ISBN 951-672-201-6.

Åström K.J. & Wittenmark B. *Computer controlled systems*. Prentice-Hall, Inc. USA. 1990. 543 p. ISBN 0-13-168600-3.

Åström K.J. & Wittenmark B. *Adaptive control*. Addison-Wesley Publishing Company, Inc. USA. 1995. 574 p. ISBN 0-201-55866-1.

Published by

Series title, number and report code of publication

VTT Publications
VTT–PUBS–498

Author(s)
Tammi, Kari

Title

Active vibration control of rotor in desktop test environment

Abstract

The goal of this work was to set up a test environment for active vibration control of rotors, to study the dynamics of the system, and to design a control system for controlling rotor vibrations. The principal idea was to use a non-contacting magnetic actuator without a load-carrying function. The test environment consisted of a desktop rotor test rig, a magnetic actuator, and a programmable control unit. The rotor was supported by conventional bearings at the ends, and the control forces were applied at the midpoint of the bearing span. The work reports modal analysis and open-loop measurement results on the test environment. The system was found to vibrate excessively when the rotor was run close to its bending critical speed at 40 Hz. Damping the system, considered as the Jeffcott rotor, by means of a velocity feedback controller was studied. The controller parameters were selected on the basis of estimates derived experimentally from the measured data. According to the simulations and experiments performed, the velocity feedback control system reduced the vibration response significantly. The controller made it possible to run the rotor across the critical speed. Another controller, a feedforward system based on an adaptive finite-impulse-response filter and the use of a reference signal, was designed to compensate disturbances caused by the mass imbalance in the rotor. The filter was adapted by the least-mean-squares algorithm. The simulations and experiments showed that the harmonic response due to the mass imbalance was successfully compensated. The use of the feedback system model improved the performance and extended the operating range of the feedforward system to super-critical conditions. The different roles of the algorithms are pointed out: feedback control increased the damping of the system, while feedforward control compensated the disturbance at the frequency of rotation. The forces required for damping the vibrations were low compared with the mass of the rotor. The use of an adaptive filter led to a considerable reduction in the response, with a minor increase in the active forces used. Results obtained elsewhere in similar test environments are also reported in this work. The data and experience acquired during the construction of the test environment are discussed.

Keywords
active vibration control, rotors, test environments, magnetic actuators, modal analysis, damping, measurements, performance, control

Activity unit

ISBN
951–38–6225–9 (soft back ed.)
951–38–6226–7 (URL:http://www.vtt.fi/inf/pdf/)

Project number
G2SU02433

Date	Language	Pages	Price
June 2003	Engl., Finnish abstr.	82 p.	B

Name of project

Commissioned by

Series title and ISSN

VTT Publications
1235–0621 (soft back ed.)
1455–0849 (URL: http://www.vtt.fi/inf/pdf/)

Sold by

VTT Information Service
P.O.Box 2000, FIN–02044 VTT, Finland
Phone internat. +358 9 456 4404
Fax +358 9 456 4374

Published by

VTT

Series title, number and report code of publication

VTT Publications
VTT–PUBS–498

Author(s)
Tammi, Kari

Title

Koelaitteiston roottorin aktiivinen värähtelynhallinta

Abstract

Työn tavoitteena oli rakentaa koelaitteisto roottorivärähtelyjen aktiivisen hallinnan tutkimukseen, määrittää laitteiston dynamiikka ja suunnitella säädin roottorin värähtelyjen vaimentamiseksi. Laitteiston käyttötarkoitus oli tutkia kosketuksettoman toimilaitteen käyttöä perinteisillä laakereilla tuetun roottorin värähtelyjen vaimentamiseen. Koelaitteisto koostui pöytäkokoisesta roottorikoelaitteesta, sähkömagneettisesta toimilaitteesta sekä ohjelmoitavasta ohjainyksiköstä. Koelaitteiston roottori oli liukulaakeroitu päistään, aktiiviset voimat kohdistettiin laakerivälin keskelle. Seuraavaksi esitellään koelaitteistolle tehdyn moodianalyysin sekä avoimen silmukan mittausten tulokset. Tulosten perusteella roottorilla todettiin olevan terävä resonanssi noin 40 Hz taajuudella. Systeemiä approksimointiin Jeffcott roottorina. Systeemin vaste vaimennettiin ensiksi suunnittelemalla takaisinkytketty säädin, jonka parametrit valittiin mitatun datan perusteella. Simuloinnit ja käytännön kokeet koelaitteistolla osoittivat, että roottorin värähtelyvaste pieneni merkittävästi säätimen ansiosta. Säätimen käyttö mahdollisti roottorin käyttämisen lähellä sen kriittistä nopeutta olevilla pyörimisnopeuksilla sallituissa värähtelyrajoissa. Toinen säädin, joka oli myötäkytketty adaptiivinen, suunniteltiin roottorin massaepätasapainosta johtuvan herätteen kompensoimiseksi. Myötäkytkettynä järjestelmänä käytettiin LMS-algoritmilla adaptoitavaa FIR-suodatinta, joka käytti kierrospulssianturilta generoitua sinisignaalia referenssi-signaalinaan. Simulointien ja käytännön kokeiden perusteella myötäkytketty algoritmi vähensi roottorin värähtelyvastetta entisestään. LMS-algoritmin versio, joka ei käytä hyväkseen vaimennettavan systeemin mallia toimi alikriittisillä pyörimisnopeuksilla. Takaisinkytketyn järjestelmän mallin lisäys laajensi myötä-kytketyn säätimen toiminta-alueen myös ylikriittisille nopeuksille lisäten myös säätimen suorituskykyä. Tutkimuksessa havaittiin algoritmien merkitykset: takaisinkytketty järjestelmä lisäsi systeemin vaimennusta ja myötäkytketty järjestelmä kompensoi herätteen tehokkaasti. Lisäksi havaittiin, että värähtelyjen vaimennus saatiin aikaan pienillä voimilla suhteessa roottorin massaan. Adaptiivisen suodattimen avulla vastetta voitiin pienentää merkittävästi voimien juurikaan kasvamatta. Työssä kuvataan koelaitteisto ja kerrotaan sen rakentamiseen liittyvät asiat. Lisäksi raportoidaan kirjallisuusselvityksen avulla löydetyt vastaavat koeympäristöt.

Keywords

active vibration control, rotors, test environments, magnetic actuators, modal analysis, damping, measurements, performance, control

Activity unit

ISBN			Project number
951–38–6225–9 (soft back ed.) 951–38–6226–7 (URL: http://www.vtt.fi/inf/pdf/)			G2SU02433
Date	Language	Pages	Price
June 2003	Engl, suom. tiiv.	82 s.	B
Name of project		Commissioned by	
Series title and ISSN		Sold by	
VTT Publications 1235–0621 (soft back ed.) 1455–0849 (URL: http://www.vtt.fi/inf/pdf/)		VTT Information Service P.O.Box 2000, FIN–02044 VTT, Finland Phone internat. +358 9 456 4404 Fax +358 9 456 4374	

VTT PUBLICATIONS

Tätä julkaisua myy	Denna publikation säljs av	This publication is available from
VTT TIETOPALVELU PL 2000 02044 VTT Puh. (09) 456 4404 Faksi (09) 456 4374	VTT INFORMATIONSTJÄNST PB 2000 02044 VTT Tel. (09) 456 4404 Fax (09) 456 4374	VTT INFORMATION SERVICE P.O.Box 2000 FIN–02044 VTT, Finland Phone internat. +358 9 456 4404 Fax +358 9 456 4374

ISBN 951–38–6225–9 (soft back ed.)
ISSN 1235–0621 (soft back ed.)

ISBN 951–38–6226–7 (URL: http://www.vtt.fi/inf/pdf/)
ISSN 1455–0849 (URL: http://www.vtt.fi/inf/pdf/)